A new synergistic model for simulating exercise incorporating control mechanisms at cellular and organ scales

Pearce, N. F. & Kim, E.

Published PDF deposited in Coventry University's Repository

Original citation:
Pearce, NF & Kim, E 2023, 'A new synergistic model for simulating exercise incorporating control mechanisms at cellular and organ scales', Computers in Biology and Medicine, vol. 163, 107141.
https://dx.doi.org/10.1016/j.compbiomed.2023.107141

DOI 10.1016/j.compbiomed.2023.107141
ISSN 0010-4825
ESSN 1879-0534

Publisher: Elsevier

This is an open access article under the CC BY license
(http://creativecommons.org/licenses/by/4.0/)

.

Computers in Biology and Medicine 163 (2023) 107141

Contents lists available at ScienceDirect

Computers in Biology and Medicine

journal homepage: www.elsevier.com/locate/compbiomed

A new synergistic model for simulating exercise incorporating control mechanisms at cellular and organ scales

Nicholas F. Pearce *, Eun-jin Kim

Fluids and Complex Systems Center, Faculty of Engineering, Environment and Computing, Coventry University, Coventry, CV1 5FB, UK

ARTICLE INFO

Keywords:
Nonlinear dynamics
Multi-scale model
Exercise
Cardiac cycle
Lumped-parameter model

ABSTRACT

The physiological response of the cardio-vascular system (CVS) to physical activity is of great importance to those working in sporting research and has profound consequences for the health and well-being of people. Coronary vasodilation and the physiological mechanisms involved in exercise have frequently been the focus of numerical models for simulating exercise. This is partly achieved using the time-varying-elastance (TVE) theory, which prescribes the pressure-volume relationship of the ventricle as a periodic function of time, tuned using empirical data. The empirical foundations of the TVE method however, and its suitability for CVS modelling are frequently questioned. To overcome this challenge, we adopt a different synergistic approach in which a model for the microscale heart muscle (myofibers) activity is embedded within a macro organ-scale CVS model. We developed such a synergistic model by including the coronary flow and various control mechanisms at the circulation level through feedback and feedforward means, and at the microscale (contractile) through the regulation of ATP availability and myofiber force depending on exercise intensity or heart rate. The coronary flow produced by the model displays the well-known 2-phase character of the flow, which is preserved under exercise. The model is tested by simulating reactive hyperemia, which is a transient occlusion of the coronary flow, successfully reproducing the additional coronary flow following the block removal. On-transient exercise results reveal a rise in both cardiac output and mean ventricle pressure as expected. The stroke volume increases initially, but then declines during the latter period of HR rise, corresponding with one of the main physiological responses to exercise. The pressure-volume loop expands during exercise, as systolic pressure rises. The Myocardial oxygen demand increases during exercise and the coronary blood supply increases in response, causing an excess of oxygen supply to the heart. Off-transient exercise recovery is largely a reverse of this response, although the behaviour is slightly more varied, with sudden spikes in coronary resistance. Different levels of fitness and exercise intensity are tested and reveal that the stroke volume rises until a level of myocardial oxygen demand is reached at which point it declines. This level of demand is independent of fitness or exercise intensity. An advantage of our model is demonstrated in the correspondence between the micro and organ scale mechanics so that cellular pathologies can be traced from exercise performance with relatively little computational or experimental expense.

1. Introduction

Understanding the cardiovascular changes that occur during exercise is an area of health research of great interest to the sporting community and is important for many areas of human health. As noted by Xiang et al. [1], exercise or physical activity is one of the most demanding responses the body makes during everyday activity. Exercising tissue requires more oxygen, placing greater demands on the heart and other organs, and one of the more pronounced responses to this increased demand is the rise in heart rate (HR) and cardiac output (CO). Many other organs also undergo changes, most of which lie hidden from human senses. See Xiang et al. [1] for a comprehensive review of these responses and the possible mechanisms involved. As an example, vasodilation occurs in exercising tissues and likewise vasoconstriction in non-exercising tissue. In this way the body regulates the blood and oxygen flow around the body as more oxygen and blood will reach exercising parts and less in the resting. Vasodilation on its own would lower the blood pressure, so the heart increases the ventricle pressure in response. As the heart pumps faster and harder, its demand increases too, so coronary vessels also dilate. ATP availability also rises during exercise to 'fuel' the rise in cellular activity [1–3]. These responses occur locally and systemically, mediated by sympathetic or parasympathetic activation. Many tests, experiments and simulations

* Corresponding author.
E-mail address: pearcen5@uni.Coventry.ac.uk (N.F. Pearce).

https://doi.org/10.1016/j.compbiomed.2023.107141
Received 4 April 2023; Received in revised form 24 May 2023; Accepted 4 June 2023
Available online 8 June 2023
0010-4825/© 2023 The Author(s). Published by Elsevier Ltd. This is an open access article under the CC BY license (http://creativecommons.org/licenses/by/4.0/).

have been conducted to gain further insight and elucidate the processes involved. Despite a growing body of research though, the mechanisms involved in responding to exercise have yet to be fully established.

The rise in the coronary demand is supplied largely by increased flow in the coronary network; the vasculature supplying the heart with blood. The flow is aided by vasodilation in coronary vessels. Feigl [4] looks at possible neural mechanisms responsible for this vasodilation, observing that sympathetic innervation at the onset of exercise anticipates increases in demand, and controls the tone of the arteries to minimise O_2 supply delay. This response can be labelled a feedforward control mechanism, as adjustments are made in 'anticipation' of future changes in demand. Feedforward adjustments are made to parts of the coronary network via neural impulses [4,5]. Feedback, in contrast to feedforward, makes adjustments according to the current state of the system and coronary supply and demand. Neural signals mediate feedforward adaptations in coronary vasculature tone via two main types of adrenoreceptors, α and β. β adrenoreceptors have long been shown to cause vasodilation and are less susceptible to 'sympathetic escape' which affects α adrenoreceptors and reduces their effect [1]. Despite this, they are still responsible for maintaining blood pressure in exercising tissues [5].

α blockade alone does not stop coronary vasodilation, but when combined with β blockade, lower aortic pressure, coronary flow, and O_2 consumption result [6] leaving many researchers to conclude that the dominant control factor for vasodilation appears to be feedback control. Increased sympathetic activity by β receptors is also responsible for elevated contractility which is responsible for increases in the stroke volume [1]. Of the numerous mechanisms postulated to be responsible for vasodilation, many are dismissed including K_{ATP} channels, nitric oxide, adenosine, and indo- and endothelin. Feedback necessarily requires an 'error signal' and a set point to compare it with. This signal is assumed to relate to the myocardial O_2 deficit; the difference between myocardial O_2 supply and demand [7,8]. Arthurs et al. [5] termed this error signal 'OSES', the myocardial oxygen supply error signal.

Computer and mathematical modelling helps investigate complex systems as it allows for system visualisation, hypotheses, and predictions to be examined [9]. There are several examples of models detailing the coronary bed in a cardiovascular system ranging in complexity and detail, with zero-dimensional (0D) electrical analogies being of the most prominent. Mantero et al. [10] develop a detailed cardiovascular lumped-parameter model which includes the coronary bed, and examine the effects of stenoses by altering the coronary vascular resistance. As illustrated by Mantero et al. a weakness of 0D (and 1D) models is their inability to account for local fluid behaviour, such as shear stresses and local pressures. Duanmu et al. [11], however, did incorporate the effect of head loss at the entrance to the large coronary artery. They used patient CT scans to create a detailed coronary network which is used as part of a 0D lumped-parameter cardiovascular model. After comparing model results with experimental data, they study the effects of stenoses. Exercise and blood flow control are not considered. The simplicity of 0D models and the absence of boundary conditions required by more detailed modelling allows results to be examined with relatively little expense.

Few numerical models of coronary blood flow control are available in the literature and those that are vary in complexity, again from 0D lumped-parameter models [5,12,13], to 3D models [14]. Barnea [12] use a simple 3 element 0D Windkessel model of the cardiovascular system, and adjust the resistance to balance the myocardial O_2 supply and consumption, in which their control method could be described as a feedback control approach. Other examples of feedback mechanisms are provided by [3,5,15]. Examples of feedforward control mechanisms are provided by [5,14]. Arthurs et al. [5] give detailed feedforward and feedback mechanisms using the instantaneous and total O_2 deficit for the feedback control and a feed-forward control mechanism similar to Kim et al. [14], where the vasodilation is controlled according to changes in demand only. The total historical O_2 deficit ensures that any shortfalls in the oxygen supply are taken into account when adjusting the coronary system. Their model of the heart and coronary system form a 0D lumped-parameter circuit, tested using a lumped parameter systemic circuit. Their model of the ventricular function makes use of the time-varying elastance (TVE) theory. Using empirical data, the TVE method tunes a periodic function of time which prescribes the pressure-volume relation of the left ventricle (LV). When used for CVS modelling, the TVE method is frequently questioned partly due to its empirical foundations [16,17] and the neglect of haemodynamic-regulating feedback mechanisms which prevents an accurate analysis of various pathologies such as fibrillation and clinical interventions. See [18,19] for further detail.

Numerical approaches to understand or simulate exercise focus almost exclusively on the mechanisms instigating coronary dilation, with little attention given to the many other CVS adaptions. This is partly due to the use of the TVE approach. This obscures the microscale dynamics preventing an investigation of the exercise adaptations at the microscale. In this report, we aim to incorporate coronary control into an expanded version of the low-order, synergistic, cardiovascular system model by Kim and Capoccia [18,19] to create a low-order CVS model capable of simulating the physiological response during exercise. Our unique approach has the advantage that the dynamics of the microscale sarcomere are embedded in macro organ-scale functions such as ventricular pressure and flow. The TVE approach and its disadvantages are therefore negated due to the model's synergism allowing for the modelling of cardiac feedback and feedforward systems. As the microscale is also modelled, the exercise-dependent microscale adaptations can be investigated. It was developed to be compact and intuitive to enable clinicians working in a demanding healthcare setting to examine the effects of cellular interventions on the pressure-volume response of the heart quickly with relative low cost. The model was validated in [18] where it was used successfully to study Left Ventricle Assist Device (LVAD) function as well as various pathologies such as dilated cardiomyopathy, and in [19,20] it was used to model the mechano-electric feedback (MEF) mechanism. MEF effects consistent with other authors were found such as longer action potential duration (APD) [21] and ectopic peaks in electrical signals along with rapid ventricular oscillation [22–24] revealing the effect of stretch activated ion channels (SACs). In [25] it was used to investigate disorders of the LV values; the aortic and mitral. Mitral valve stenosis caused a reduction in EDV and ESV magnitude consistent with [26]. For example the EDV shifts left by 7 ml, and the ESV left by 1.5 ml whilst [6] saw a shift of 5 ml and 3 ml in the EDV and ESV respectively for a similar stenosis severity range. Regurgitation results agreed with medical reports [27]. Results for aortic valve disorders also agreed well with published data [28].

The remaining parts of this paper are laid out as follows: in Section 2 the CVS model is described along with the heart rate model [29,30], and cardiac control. Results follow in Section 3, in which reactive hyperemia, the heart rate model, and both on and off transient exercise are tested. The results are discussed and explored in Section 4, and Section 5 provides a conclusion.

2. Methods

In this section, we propose a new CVS cardiovascular model to include coronary flow dynamics and various feedback mechanisms involved in exercise. Specifically, the synergistic CVS model from [18,19] is expanded to include the coronary tree and additional systemic elements. The coronary network design by Arthurs et al. [5] is adopted as it has a relatively compact design, whilst allowing a fine control over different parts of the network. A further advantage of the synergistic model here is that in addition to the coronary vasodilation, other physiological system changes can be modelled, such as the increased ATP availability or rise in active ventricle contraction force [1].

2.1. Microscale mechanical model

To simulate the sarcomere and myofiber mechanics, [18] uses the BCS formulation [31,32]. This captures the behaviour of the collective actin–myosin at work in the left ventricle. The BCS formulation is based around a Hill-Maxwell rheological design, in which an electrically activated contractile element is modelled in series with another elastic element allowing active relaxation. These two series elements express the active sarcomere dynamics. A third, passive elastic element representing the collagen surrounding the sarcomere sits parallel to the series elements. Eqs. (1) to (4) govern the velocity v_c, strain ϵ_c, stress τ_c, and stiffness k_c of the myofiber element. The 'c' subscript denotes that it is the contractile part. The subscript + of u_+ means that it takes a non-zero value only when $u > 0$ (i.e. + represents a Heaviside function). Eq. (6) is the force from the passive element σ_p and is assumed to be exponential [33].

$$\frac{dv_c}{dt} = -\chi v_c - \omega_0^2 \epsilon_c - a\tau_c d_0(\epsilon_c) + b\left(\sqrt{\frac{V}{V_0}} - 1\right) \tag{1}$$

$$\frac{d\epsilon_c}{dt} = v_c \tag{2}$$

$$\frac{d\tau_c}{dt} = k_c v_c - (\alpha_l |v_c| + |u|)\tau_c + \sigma_0 u_+ \tag{3}$$

$$\frac{dk_c}{dt} = -(\alpha_l |v_c| + |u|)k_c + k_0 u_+ \tag{4}$$

$$d_0(\epsilon_c) = e^{-\beta_0(\epsilon_c - \Psi)^2} \tag{5}$$

$$\sigma_p = \frac{k_2}{k_1}[\exp(k_1(\sqrt{V/V_0} - 1)) - 1] \tag{6}$$

In Eq. (1), χ is a damping parameter and ω_0 is the sarcomere oscillation frequency. a and b are parameters for the active and passive forces respectively. The first term on the RHS ($-\chi v_c$) represents a damping force; the next term ($\omega_0^2 \epsilon_c$) represents a harmonic force; $a\tau_c d_0(\epsilon_c)$ is an active force; and $b\left(\sqrt{\frac{V}{V_0}} - 1\right)$ is a passive force. α_l in Eqs. (3) and (4) is another damping parameter, and u represents the time-varying calcium bound Troponin-C concentration responsible for cell activation [34]. σ_0 and k_0 are the maximum sarcomere active stress and stiffness respectively. k_1 and k_2 are parameters for the passive force function in Eq. (6). The Eq. (5) for $d_0(\epsilon_c)$ represents the Frank-Starling effect of cell stretching, where Ψ is a constant off-set parameter that controls the cellular contractility, i.e. by how much does cell stress translate to strain. V_0 is a reference volume parameter. Eq. (6) and the last term in Eq. (1) are based on a contracting cylinder with constant height [31], which gives strain proportional to the square root of the ventricle volume V, i.e. $\epsilon_c \sim V$. The last term in Eqs. (3) and (4) represents the chemical activation of the cell due to chemical input ($u > 0$), and $(\alpha_l |v_c| + |u|)$ represent deactivation.

2.2. Macroscale ventricle pressure

The macroscale ventricle pressure P_v is governed by Eq. (7) below. This equation expresses how the collective cellular elements determine the organ-scale dynamics.

$$P_v = \Gamma \frac{V_0}{V}[d_0(\epsilon_c)\tau_c + \sigma_p], \tag{7}$$

where Γ is the ratio of ventricular wall thickness to the radius.

2.3. Expanded circulation model

We expand our previous works [18,19] to include the coronary circulation, and present the electrical-equivalent diagram of the complete model in Fig. A.1 in the appendix. The top branch on the right is the coronary tree and the bottom branch is the systemic. Eqs. (8) to (17) below govern the flow around the various parts of our model. Here, m is the aortic pressure, F_a is the aortic flow, P_r is the left atrial pressure, and P_s is the systemic pressure. P_{ac} and P_{sp} are the coronary arterial pressure and systemic proximal pressure. P_h in Eq. (9) is introduced for notational convenience. Q_{cor} is the coronary flow and V is the volume.

$$P_{im} = P_{im}^* + P_v \tag{8}$$

$$P_h = \left(R_{sp}F_a + P_{ac}\frac{R_{sp}}{R_{ac}} + P_{sp}\right)\left(\frac{R_{ac}}{R_{sp} + R_{ac}}\right) \tag{9}$$

$$Q_{cor} = \frac{P_h - P_r}{R_{ac} + R_{pc} + R_{dc}} \tag{10}$$

$$\frac{dV}{dt} = \frac{1}{R_m}(P_r - P_v)_+ - \frac{1}{R_a}(P_v - m)_+ + C_{im}\frac{dP_{im}^*}{dt} \tag{11}$$

$$\frac{dm}{dt} = -\frac{F_a}{C_a} + \frac{1}{C_a R_a}(P_v - m)_+ \tag{12}$$

$$\frac{dF_a}{dt} = \frac{m - P_h}{L_s} - \frac{R_c F_a}{L_s} \tag{13}$$

$$\frac{dP_{ac}}{dt} = \frac{1}{C_{ac}R_{ac}}(P_h - P_{ac}) - \frac{1}{C_{ac}R_{pc}}(P_{ac} - P_{im}) \tag{14}$$

$$\frac{dP_{im}^*}{dt} = \frac{1}{C_{im}R_{pc}}(P_{ac} - P_{im}) - \frac{1}{C_{im}R_{dc}}(P_{im} - P_r) \tag{15}$$

$$\frac{dP_{sp}}{dt} = \frac{1}{C_s R_{sp}}(P_h - P_{sp}) - \frac{1}{C_s R_s}(P_{sp} - P_r) \tag{16}$$

$$\frac{dP_r}{dt} = \frac{1}{C_r R_s}(P_{sp} - P_r) + \frac{1}{C_r R_{dc}}(P_{im} - P_r) - \frac{1}{C_r R_m}(P_r - P_V)_+ \tag{17}$$

Eq. (8) for the intramyocardial pressure P_{im} is updated after each calculation and used as an input for the next, similar to the ventricle pressure P_v. Again, the subscript '+' denotes the use of only positive values of the corresponding term. R_m, R_a, R_c, and R_s above are the aortic, atrial, characteristic, and systemic resistances respectively. C_a, C_r, and C_s are the aortic, left atrial, and systemic compliances. L_s is the blood inertia. We note that R_{pc}, similar to Arthurs et al. [5], is the resistance of the proximal coronary vessels and R_{dc} is the distal. R_{ac} is the (constant) coronary arterial resistance. In this paper, R_{pc} and R_{dc} are not necessarily constant, but are varied to model coronary vasodilation. R_{sp} and R_s are the (constant) proximal systemic and systemic resistances respectively. The subscript of the compliance, C, denotes the corresponding resistance parameters i.e. C_{ac} corresponds to R_{ac}. Tables 1 and 2 give the variable definitions and the value of the constants for a healthy person at rest. The values of R_{dc} and R_{pc} provided in Table 2 are used for the resting state. They vary away from this value when coronary vasodilation is required.

2.4. Electro-chemical model

The cellular electrical messaging activity in response to deformation is modelled using a FitzHugh–Nagumo [35] formulation and represented by Eqs. (18) to (20) below. The electrical activity drives cell activation and deactivation through the chemical u activity described above; see equations ((3), (4)).

$$\frac{dp}{dt} = 0.1(q - p + \mu_1 \tau_c) \tag{18}$$

$$\frac{dq}{dt} = 10q(1 - q^2) - 10(2\pi)^2 p + 20\cos(2\pi \cdot HR \cdot t) \tag{19}$$

$$u = \alpha_u q \tag{20}$$

p and q model the slow and fast electrical signals respectively. $20\cos(2\pi \cdot HR \cdot t)$ is an oscillating force which mimics the signals originating from the SAN node. A frequency 1 Hz ($HR = 1$) is used to represent a resting heart rate. α_u is a positive proportional constant which will be varied to model ATP availability variation during exercise [1,2,36]. μ_1 is a positive constant which represents the mechano-electric effect; the influence of mechanical stretch on the electrical action potential. See [18–20] for further detail regarding the MEF and the meaning of μ_1 in the model. Again, tables 1 and 2 give the physiological meanings of all model variables and the resting steady state case parameter values.

Table 1
Variables and their physiological meaning.

Variable	Physiological description
v_c	velocity of the contractile element (s^{-1})
ϵ_c	Strain of the contrile element
τ_c	Active tension of the contractile element (mmHg)
k_c	Stiffness of the contractile element (mmHg)
σ_p	Passive stress (mmHg)
u	Chemical activity (s^{-1})
p	Slow electric variable
q	Fast electric variable
P_v	Left ventricular pressure (mmHg)
P_r	Atrial pressure (mmHg)
P_h	Pressure exiting heart (mmHg)
P_{ac}	Coronary artial pressure (mmHg)
P_{pc}	Coronary proximal pressure (mmHg)
P_{dc}	Coronary distal pressure (mmHg)
P_{im}	Intramyocardial pressure (mmHg)
P_{im*}	Temporary intramyocardial pressure (mmHg)
P_{sp}	Systemic distal pressure (mmHg)
P_{cor}	The coronary pressure (mmHg)
Q_{cor}	The coronary flow (ml)
V	Left ventricular volume (ml)
m	Aortic pressure (mmHg)
H	O_2 surplus/deficit (ml)
$\overline{H}$	Cumulative O_2 surplus/deficit (ml)
$M\dot{V}O_2$	Myocardial O_2 demand

2.5. Modelling the heart rate during exercise

Representation of exercise involves increasing the heart rate similar to [5]. Unlike [5] however, we use a physiological representation of the heart rate during exercise. Instead of continuously changing the heart rate in time, in this paper we change it discretely after every complete cardiac cycle (see Section 3.1 for the definition of a cycle). Furthermore, the model proposed in [29,30] is adopted to prescribe both the on-transient initial rise in heart rate at the start of exercise and the off-transient recovery. Based on the established 3-phase model [37], it is simple to model yet captures the physiological features of exercise. The 3-phase model simulates the three oxygen uptake phases observed during any constant activity intensity input. In this model, HR in Eq. (19) varies according to Eq. (21) below (see also Eqs. (36)–(51) for details).

$$\frac{dHR}{dt}(HR, HR(0), \lambda, v, t) = -f_{min} f_{max} f_D \tag{21}$$

$HR(0)$ is the initial heart rate; λ quantifies the patient cardiovascular condition with $\lambda = 1$ being excellent, $\lambda = 0$ being the worst, and $0 \leq \lambda \leq 1$; $f_{max}(HR)$ depends on the heart rate only; $f_{min}(HR, \lambda)$ depends on the heart rate and λ; $f_D(HR, HR(0), v, \lambda, t)$ depends on HR and $HR(0)$, the exercise level v (given in Km/h), λ, and time t. f_{max} (Eq. (36)) and f_{min} (Eq. (37)) govern the HR dynamics near the maximum and minimum HR, and f_D (Eq. (38)) governs the HR dynamics near the body's circulatory O_2 demand D (Eq. (45)). f_{max}, f_{min}, f_D, and D are provided in the appendix. v in Eq. (48) can be any prescribed function of time. In the model, there are two minimum heart rates: a female in Eq. (40) and a male in Eq. (39). The former is used in this paper. See [29,30] for a fuller discussion regarding the heart rate behaviour and the HR model. The HR in bps produced by the heart rate model is used in place of the SAN frequency element in Eq. (19).

2.6. Cardiac control at the circulation level

We propose a model where the cardiac adaptation to exercise is incorporated at each heart cycle $c = 1, 2, 3, \ldots$ rather than continuously in time. To this end, we define the following measures defined over each cycle c:

$$\overline{Q_{cor}}(c) = \int_{t_c}^{t_{c+1}} Q_{cor}(t)dt, \tag{22}$$

$$\overline{P_{cor}}(c) = \int_{t_c}^{t_{c+1}} P_{cor}(t)dt, \tag{23}$$

$$MVO_2(c) = \int_{t_c}^{t_{c+1}} M\dot{V}O_2(t)dt, \tag{24}$$

$$H(c) = \Phi MVO_2(c) - \gamma^{-1}\overline{Q_{cor}}(c), \tag{25}$$

$$\overline{H}(c) = \overline{H}(c-1) + H(c) \tag{26}$$

Each time integration is performed over a single cycle c, starting at t_c and ending at t_{c+1}. Q_{cor} (ml) is the coronary flow (pressure drop across the coronary network divided by the coronary network resistance), P_{cor} (mmHg) is the coronary pressure, $M\dot{V}O_2$ (ml) is the myocardial O_2 demand, H (ml) is the O_2 surplus/deficit, γ is the extractable oxygen proportion of the coronary blood, and Φ is a constant which ensures the deficit H is zero at rest. $\overline{H}(c)$ (ml) is the accumulated oxygen deficit. The evidence that the historical accumulated O_2 deficit $\overline{H}$ exists and is important for myocardial oxygen control can be easily observed in the response to situations such as hyperemia [5]. The values of the constants γ and Φ are given in Table 2 in the appendix. $MVO_2(c)$ is calculated here in a similar manner to [5,12]; that is, using the physiological observation that the pressure-volume-area (PVA) of a cardiac cycle (Joules) follows the myocardial O_2 demand $MVO_2(c)$ [38], with the assumption that 1 ml of O_2 provides 20 J. At rest, $\overline{Q_{cor}}(c) = 0.89$ ml/beat, $\overline{P_{cor}}(c) = 142.7$ mmHg, $MVO_2(c) = 1.05$ ml/beat, and $H(c) = \overline{H}(c) \approx 0$ ml.

Coronary control during exercise involves lowering the coronary resistance parameters R_{pc} and R_{dc}. In comparison, R_{ac} is held constant as are the systemic resistances R_s and R_{sp}. Here, similar functions to [5] are used for the coronary resistance control of R_{dc}, given in Eqs. (27) and (28) below. These are simpler than those used in [5], who implement cardiac control continuously with time, as the resistance here is changed only after a complete cardiac cycle, when $MVO_2(c)$ is available. Specifically, for $c = 1, 2, \ldots$ $R_{dc}(c)$ and $S_{pc}(c-1)$ are calculated by

$$R_{dc}(c) = aa_1 \frac{\overline{P_{cor}}(c-1)}{S_{dc}(c-1)}, \tag{27}$$

$$S_{dc}(c-1) = \overline{Q_{cor}}(c-1) + g_b\gamma^{-1}\overline{H}(c-1)_+ + g_{ff1}\gamma^{-1}\left[\frac{MVO_2(c-1)^2}{MVO_2(0)}\right] \tag{28}$$

g_b and g_{ff1} are the feedback and feedforward gains respectively. aa_1 is a constant which yields $R_{dc}(0) = aa_1\frac{\overline{P_{cor}}(0)}{S_{dc}(0)}$, where $R_{dc}(0)$ and aa_1 are values for the resting heart given in Table 2, and S_{dc} is the coronary flow and additional feedforward/feedback flow elements. The values of the two gains are constants, tuned manually to produce physiologically representative results. The resistance R_{dc} is decreased if the total oxygen deficit $\overline{H}$ is positive and increasing. For the last term in S_{dc}, the square of the demand is used to accentuate its feedforward behaviour. To model the proximal resistance R_{pc}, a similar version of the feedforward operation used by [5] is used.

$$R_{pc}(c) = aa_2 \frac{\overline{P_{cor}}(c-1)}{S_{pc}(c-1)}, \tag{29}$$

$$S_{pc}(c-1) = \overline{Q_{cor}}(0) + g_{ff2}\gamma^{-1}\left[\frac{MVO_2(c-1)^2}{MVO_2(0)}\right], \tag{30}$$

where aa_2 serves a similar purpose as aa_1 and g_{ff2} is the second feedforward gain parameter tuned to produce physiological results. It can be seen that the last term in Eq. (30) is the same as that used in Eq. (28). Similarly to $R_{dc}(0)$, $R_{pc}(0)$ and aa_2 are the values for the resting heart and are provided in Table 2.

2.7. Cardiac control at the contractile level

Due to the synergism of the model, other cardiac responses can be controlled even at the microscale level in addition to the circulation

Table 2
Resting steady state case model parameters.

Parameters	Value	Physiological meaning
R_a	0.001 mmHg s/ml	Aortic valve resistance
R_m	0.005 mmHg s/ml	Mitral valve resistance
R_c	0.0398 mmHg s/ml	Characteristic resistance
R_{sp}	0.005 mmHg s/ml	Systemic proximal resistance
R_s	0.5 mmHg s/ml	Systemic distal resistance
R_{pc}	80 mmHg s/ml	Coronary proximal resistance
R_{dc}	80 mmHg s/ml	Coronary distal resistance
R_{ac}	0.05 mmHg s/ml	Coronary arterial resistance
C_a	0.08 ml/mmHg	Aortic compliance
C_r	15 ml/mmHg	Atrial compliance
C_{ac}	0.01 ml/mmHg	Coronary arterial compliance
C_{im}	0.001 ml/mmHg	Intramyocardial compliance
C_s	1.33 ml/mmHg	Systemic compliance
σ_0	240 kpa	Maximum sarcomere active tension
k_0	120 kpa	Maximum sarcomere active elastance
k_1,	0.002 kpa	Model parameters for passive tension
k_2	14 kpa	Model parameters for passive tension
χ, α_l	100 s^{-1}, 10 m^{-1}	Sarcomere damping parameters
ω_0	100 s^{-1}	Sarcomere microscale oscillation frequency
a, b	100 m s^{-2} kpa^{-1}, 6000 m s^{-2}	Active and passive force parameters
β_0	$\frac{40}{3}$ ml^{-2}	Length-tension parameter
Γ	0.6	P_V parameter
V_0	$\frac{144}{1.5}$ ml	Volume parameter
μ_1, μ_2	0.0024 kpa^{-1}, 0 $(s\ ml)^{-1}$	MEF parameters
α_u	5 s^{-1}	Chemical-electric coupling parameter
γ	0.125	Coronary blood O_2 proportion
Φ	0.1053	O_2 surplus/deficit parameter
aa_1	3.47	
aa_2	3.46	
g_{ff1}	5/8	Feedforward gain 1
g_{ff2}	5/8	Feedforward gain 2
g_b	15/8	Feedback gain
cc	0.2	k2 gain
dd	0.375	au gain
ee	0.3	a gain
ff	5	Ψ gain

level, such as the coronary resistance discussed above. This synergistic approach will help us create a more physiologically analogous model and allows analysts working in sport research to explore cardiac function more fully. One such microscale control mechanisms is the ATP availability, which increases during exercise as noted in Section 1. This response is modelled here by modifying the chemical variable u in the microscale mechanical model through the value of the α_u parameter in Eq. (20). Increasing α_u increases the value of u. ATP availability is released by sympathetic nerve terminals in an intensity-dependant manner [1]. As a nervous system equivalent of sympathetic nerve terminals is not available, the heart rate is used instead as this is controlled (mainly) neurologically and can be used as a measure of exercise intensity. Further as noted in Section 1, the force developed by the heart increases during exercise to compensate for the vasodilation. In the model, the parameter a in Eq. (1) in the micro-scale model controls the active force developed by the ventricle myofibers. Lowering a has the effect of increasing the active force and as a consequence, ventricular ejection force. a is also controlled using the heart rate.

It will be seen that during the increase in heart rate, the stroke-volume reduces, end-diastolic volume (EDV) falls and the end-systolic volume (ESV) rises. During exercise though, the stroke volume should increase [39] at least initially as the EDV rises. The ESV remains largely unaltered [1]. The rise in stroke volume is therefore due to increases in EDV, partly due to an increased contractility. In the model presented here, it is noted that a smaller value of the passive stress parameter k_2 increases the stroke-volume by increasing the EDV. Lower k_2 effectively reduces the passive stress, which stops the heart exceeding its limits [34]. Alternatively, the systemic resistances R_{sp} or R_s could be increased, causing a rise in venous return and stroke volume, but here R_{sp} and R_s are held constant. k_2 is also controlled using the heart rate. The last exercise response using the heart rate is the contractility. An increase in ventricular contractility is a well known cardiac response to exercise and helps to increase the heart output by increasing the output volume for any given pressure. To increase the contractility in the model, the function off-set Ψ in the exponential function d_0 in Eq. (5), representing the Frank-Starling law, is decreased. Specifically, we use the following equations to prescribe the cardiac control of a, α_u, Ψ, and k_2 using the heart rate HR in bps.

$$k_2(c) = k_2(0)\exp\left[-cc\,(HR(c-1)-1)\right], \tag{31}$$

$$\alpha_u(c) = \alpha_u(0)\exp\left[dd\,(HR(c-1)-1)\right], \tag{32}$$

$$a(c) = a(0)\exp\left[-ee\,(HR(c-1)-1)\right], \tag{33}$$

$$\Psi(c) = \Psi(0)\exp\left[-ff\,(HR(c-1)-1)\right] \tag{34}$$

Here cc, dd, ee, and ff are constants that control the magnitude of the change. Their values are again tuned manually to produce physiological results. Table 2 gives their (healthy subject at rest) values.

The system of Eqs. (1) to (34) are solved in Matlab using a fourth-order Runge–Kutta scheme and the accuracy of the numerical solution is checked by systematically reducing the time-step until differences between results become negligible. Fig. 1 below illustrates this procedure, reducing the time step from $\Delta t = 2.5e^{-4}$ s to $1e^{-5}$ s and its effect on the pressure-volume loop. Although the loops appear to be identical, focusing on the top left corner (figure B) reveals small differences between results as the time-step is reduced. Between $\Delta t = 2.5e^{-4}$ s and $1e^{-4}$ s, the percentage change in mean pressure is 0.02% and between $1e^{-4}$s and $1e^{-5}$s the percentage difference is 0.0075%. As the computational time is much longer when the $\Delta t = 1e^{-5}$ compared to $\Delta = 1e^{-4}$, but from $\Delta t = 2.5e^{-4}$ to $\Delta = 1e^{-4}$ the computational reduction is not so great, $\Delta t = 1e^{-4}$ is used for this study. The values found in [31,32,34] are used for σ_0, k_0, k_1 and k_2. The values R_a, R_m, R_c, C_s, and C_a are taken from [40]. Atrial compliance C_r is adjusted to accommodate the increase in model size due to the added coronary and systemic

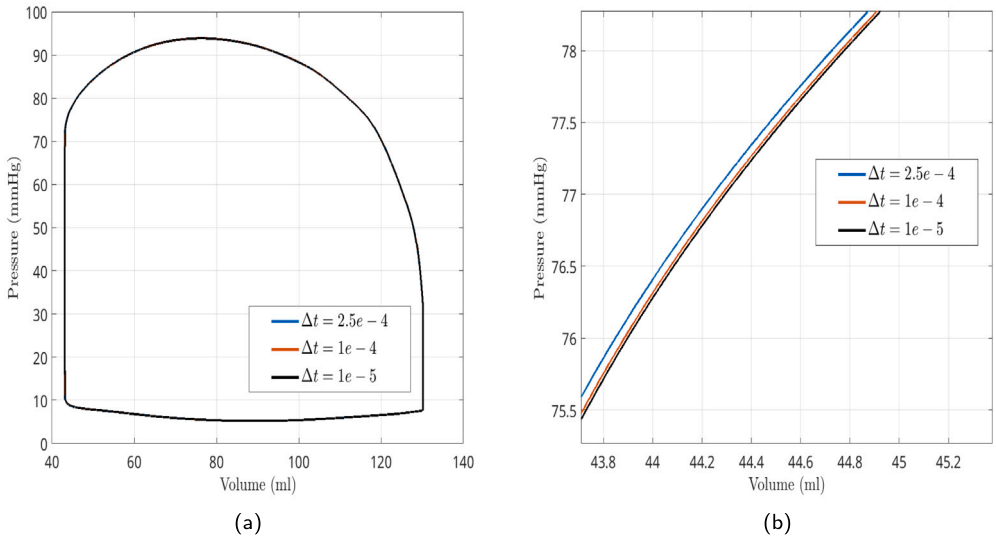

Fig. 1. The effect of the time-step on the steady-state controlled response. Fig. 1(a) shows the (steady) pressure-volume loops using 3 different time-steps, and Fig. 1(b) shows a close up of the top left corner. The effect of the time-step on the model results are clear when $\Delta t = 2.5e^{-4}$ compared to the other two time-step sizes.

elements. The remaining microscale model parameters for the resting steady state case; χ, α_l, ω_0, a, b, β_0, Γ, V_0, $\mu_{1,2}$, Ψ, and α_u are those used by [18–20,25]. The coronary and systemic resistances and compliances are all adjusted here to create a physiological representation of the pressure-volume relationship.

3. Results

3.1. Resting steady state case

The system of Eqs. (1) to (33) are first solved for a resting person free of pathologies, described here by the parameters in Table 2 and $HR = 1$. The time evolution of V and ϵ_c, τ_c and k_c, p and q, and the ventricle pressure volume loop are shown in Fig. B.1 in the appendix. The stroke volume in the resting steady state case is 87.1 ml, and the power is 0.9 W. Fig. B.2, also in the appendix, shows the steady pressure-volume loops for differing initial preloads: $V(0) = [1.0, 0.9.0.8, 0.7, 0.6]V_0$. The black line represents the end-systolic pressure-volume relationship, which shows the maximum ventricle pressure developed for any volume. Proper development of the ESPVR is an important test that the ventricular pressure-volume relationship is being modelled correctly. Improper ESPVR development is a sign of an invalid mathematical model, or clinically a possible sign of underlying abnormality. Compared with our previous works [18,19] the results here have a similar mean ventricular pressure $\overline{P_v}$ (mmHg) per heart beat, but a slightly lower stroke volume (87.1 ml here vs 92.6 ml). Here, the mean ventricle pressure $\overline{P_v}$ (mmHg) is defined as the average ventricle pressure developed during a single heart beat. The pressure-volume (PV) loop here appears to have shifted slightly to the left too i.e., with lower EDV and ESV.

3.2. Coronary flow

Fig. 2 shows the resting coronary flow produced by the model. The double-phase nature which characterises the coronary flow wave-form [5,10,11,41,42] is reproduced. This nature is preserved under exercise as it should [5]. Fig. 2(b) compares the coronary flow with the ventricular and aortic pressures. The peak in flow occurs during early diastole and reduces during systole, again reproducing the previous results in [10,42]. The magnitude of our coronary flow is of physiological order as well, although our resting flow is slightly lower than others. For example [10] show coronary flow fluctuates between 0 and 4 to 6 (depending on the coronary compliance). Here it is between 0.3 s to 1.3 ml/s. [42] however, observe coronary flows between approximately 0 and 1 ml/s in canines. [5] also found a similar magnitude in coronary flow.

Fig. 3 compares the effect of the compliance parameters C_{ac} and C_{im} on the coronary wave-form. A rise in the coronary arterial compliance C_{ac} is seen to increase the systolic flow and decrease the flow during ventricular diastole, consistent with the previous work in [10]. The intra-myocardial compliance C_{im} has the opposite effect, so an increase in the compliance reduces the diastolic coronary flow, and vice-versa for compliance reduction. The size of the resistance parameters largely just adjusts the magnitude of the coronary wave-form.

3.3. Heart rate during exercise

In this section, the heart rate model described in Section 2.5 is tested. It is found that due to the non-linear behaviour of the FitzHugh–Nagumo model given by Eqs. (18) to (20) the output heart rate (frequency) differs from the input value (HR in the SAN term in Eq. (19)). During the on-transient period for example, the model output overestimates the frequency used in the sinusoidal SAN term in Eq. (19), and an 'overshoot' in HR during the transient results. To try to compensate for this, the parameter $d(\lambda)$ in Eq. (44) in the HR model in Section 2.5 is taken to be $d(\lambda) = 0.01\lambda$ instead of $d(\lambda) = 0.08\lambda$ as was used in previous works [29,30]. This reduces the gradient of the transient behaviour in the model [29,30]. Reducing $d(\lambda)$ further prolongs the transient period and the time to reach the final HR. The resulting on-transient and off-transient exercise regimes in Fig. 4 show both the input frequency and output, highlighting the difference between the two. These results were produced using a resting heart rate of 60 beats per minute (bpm), a fitness of $\lambda = 0.85$, a constant $\upsilon = 10$ and $\upsilon = 3$, each with different starting heart rates. For on-transient exercise, $\upsilon = 10$ is chosen to maximise HR, whilst minimising any overshoot in HR. For the recovery exercise regime, $\upsilon = 3$ is chosen and not zero so that the resulting heart rate HR is close to 60 bpm. These two regimes are used to test cardiac adaptations during exercise. Other values of λ and υ are explored later in Section 3.9.

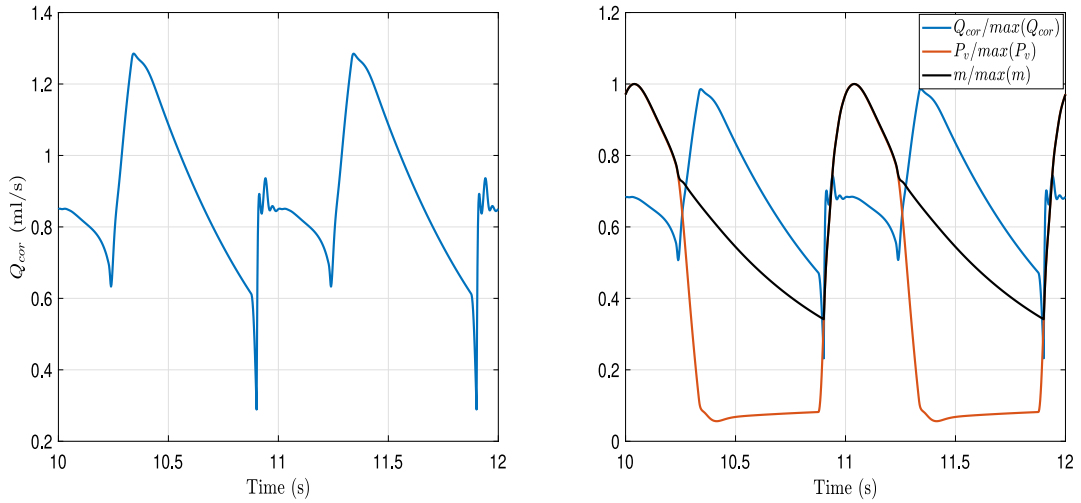

(a) Resting coronary flow during two heart cycles.

(b) Normalised coronary flow (blue) compared with the normalised ventricular (red) and aortic (black) pressures.

Fig. 2. Coronary flow: (a) The resting coronary flow during two cardiac cycles; (b) Normalised coronary flow compared with ventricular and aortic pressures.

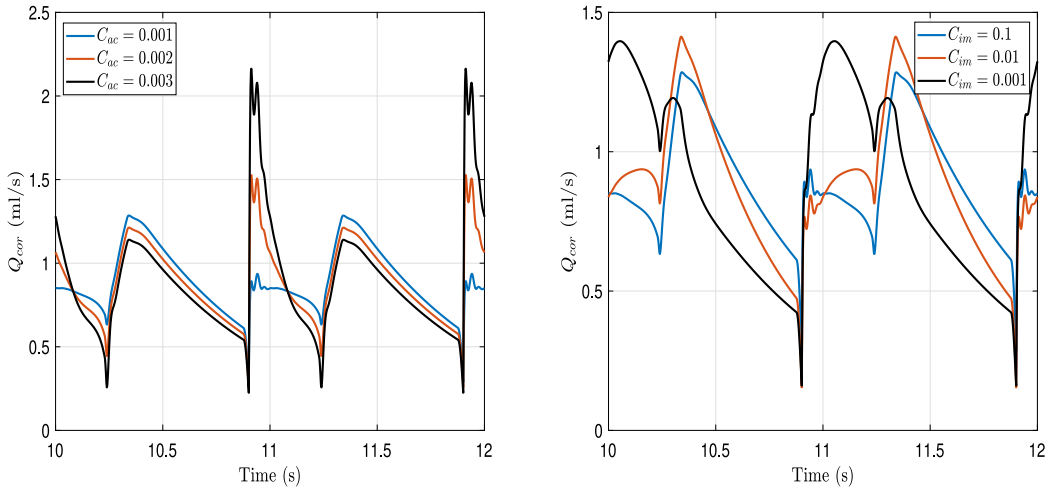

(a) The effect of the coronary arterial compliance C_{ac} on the coronary waveform.

(b) The effect of the intramyocardial compliance C_{im} on the coronary waveform.

Fig. 3. The effect of the coronary compliance and intra-myocardial compliance parameters.

3.4. The CVS model without cardiac control introduced in Sections 2.7 and 3.1

Using the on-transient exercise regime described in Sections 2.5 and 3.3 and characterised by the heart rate shown in Fig. 4(a), an exercise test without cardiac control introduced in Sections 2.7 and 3.1 is performed to highlight the failure of the model without cardiac control to simulate exercise and thus demonstrate the importance of cardiac control. Fig. 5(a) shows the pressure-volume relationship at the start (following removal of any initial transient effects) and end of the test. As can be seen, the final pressure-volume loop is smaller than the initial loop. Fig. 5(b) shows the reduction in stroke-volume (SV). Fig. 5(c) shows how the mean ventricle pressure $\overline{P_v}$ (mmHg) and cardiac output (CO) (l/min) of each heart cycle behave over increasing cycles. Despite the initial increase in both pressure and output, the CO starts to decline as the heart rate plateaus. The mean pressure increases throughout though. The rise in CO initially is solely due to the initial rise in heart rate ($CO = HR \times SV$).

3.5. Reactive hyperemia simulation using our cardiac control model

A simple test of the model with cardiac control detailed above in Section 3.1–2.7 is reactive hyperemia. Reactive hyperemia is an increase in blood flow following a temporary interruption of arterial flow. One example of this is a transient occlusion or block of coronary flow [43]. This can be modelled here by holding the coronary flow Q_{cor} at zero for a short time; a method also used by [5] for the same purpose using a period of 8 s for the coronary block. We repeat this test here by setting the coronary flow to zero i.e. $Q_{cor} = 0$ for 8 s. The results are provided in Fig. 7. The block occurs at $t = 100$ and ends at $t = 108$. Our results for coronary flow and resistance agree well with those in [5,43–45]. They may be compared with [44] reproduced in figure (Fig. 6). As can be seen the pattern of coronary flow is identical to that found here. The block of coronary flow lasted over 12 s instead of the 8 s used in this study. The myocardial blood supply is also replenished after a similar period of time too (approximately 60 s as opposed to 50 found

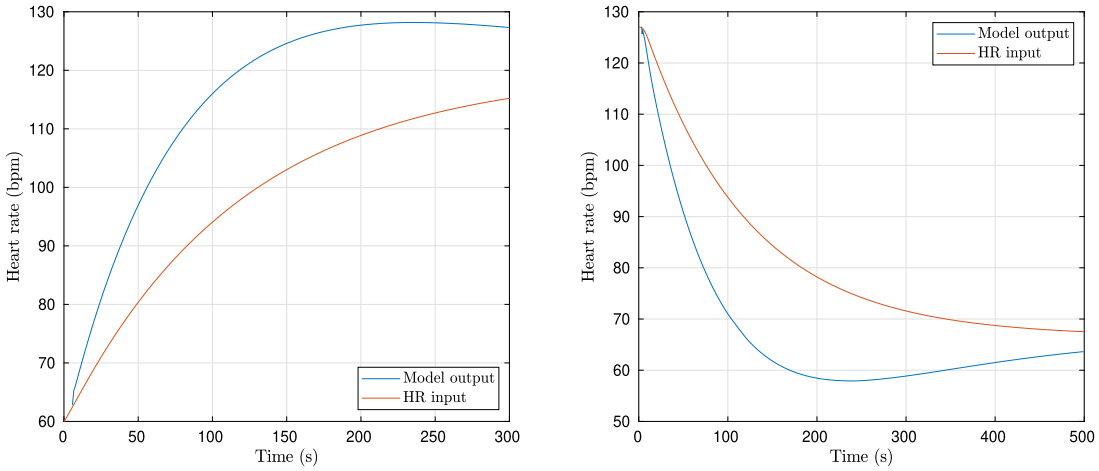

(a) On-transient exercise regime (b) Off-transient exercise regime

Fig. 4. The on and off-transient exercise regimes showing the difference between input frequency (red) and model output (blue): $\lambda = 0.85$, $HR_{rest} = 60$, $\upsilon = 10$ (Fig. 4(a)), $\upsilon = 3$ (Fig. 4(b)).

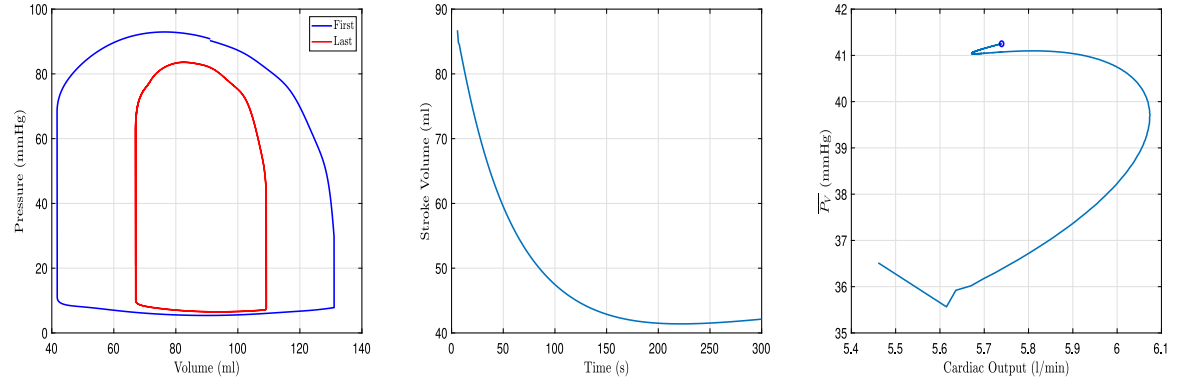

(a) The PV loop at the start (blue) and end (red) of the exercise regime (b) The decline in stroke volume (c) The resulting pump-chart without cardiac control. Marker 'o' shows the line end.

Fig. 5. The resulting response to the exercise regime shown in Fig. 4(a) without cardiac control.

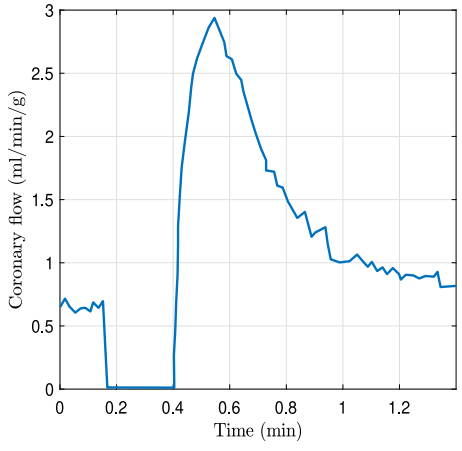

Fig. 6. The coronary flow response to a flow blockage of around 12 s.
Source: This figure is a reproduction of Fig. 2D in [2].

here). Olsson too observed a debt-repayment period of approximately 40 s in canines. Arthurs et al. (2016) observed only a 10 s period until most of the blood was repaid. Fig. 7(a) shows the total cycle coronary flow reducing to zero during the block, then rising above the resting coronary flow after the block is lifted. The reason for the increase following the block is to make up the deficit incurred during the block. The duration of the coronary flow rise lasts longer than the block and shows a more gradual decline. The parameter g_b controls the character (shape) of the flow. $g_b = 15/8$ was used to produce the results in Fig. 7.

Fig. 7(b) shows the coronary resistances R_{pc} and R_{dc}. When the block occurs, R_{dc} falls, then gradually rises again. It stays at a reduced value after the block is lifted to increase the coronary flow following the occlusion. R_{pc} fluctuates slightly but is largely unaffected by the flow block as the demand during this period is barely altered. This is consistent with the finding in [5,44] which show that only the metabolic control system is activated by the occlusion. Fig. 7(c) shows the coronary deficit per cardiac cycle H and the total historical deficit $\overline{H}$ is shown in Fig. 7(d). When the block occurs, the deficit H rises and stays high until the block ends. It then falls and becomes negative due to the additional coronary blood flow required to make up for deficit incurred during block. It rises again to 0 after the O_2 deficit is repaid. The mean ventricular pressure (not shown) falls slightly as does the aortic pressure m as noted in [45] too. Our model however

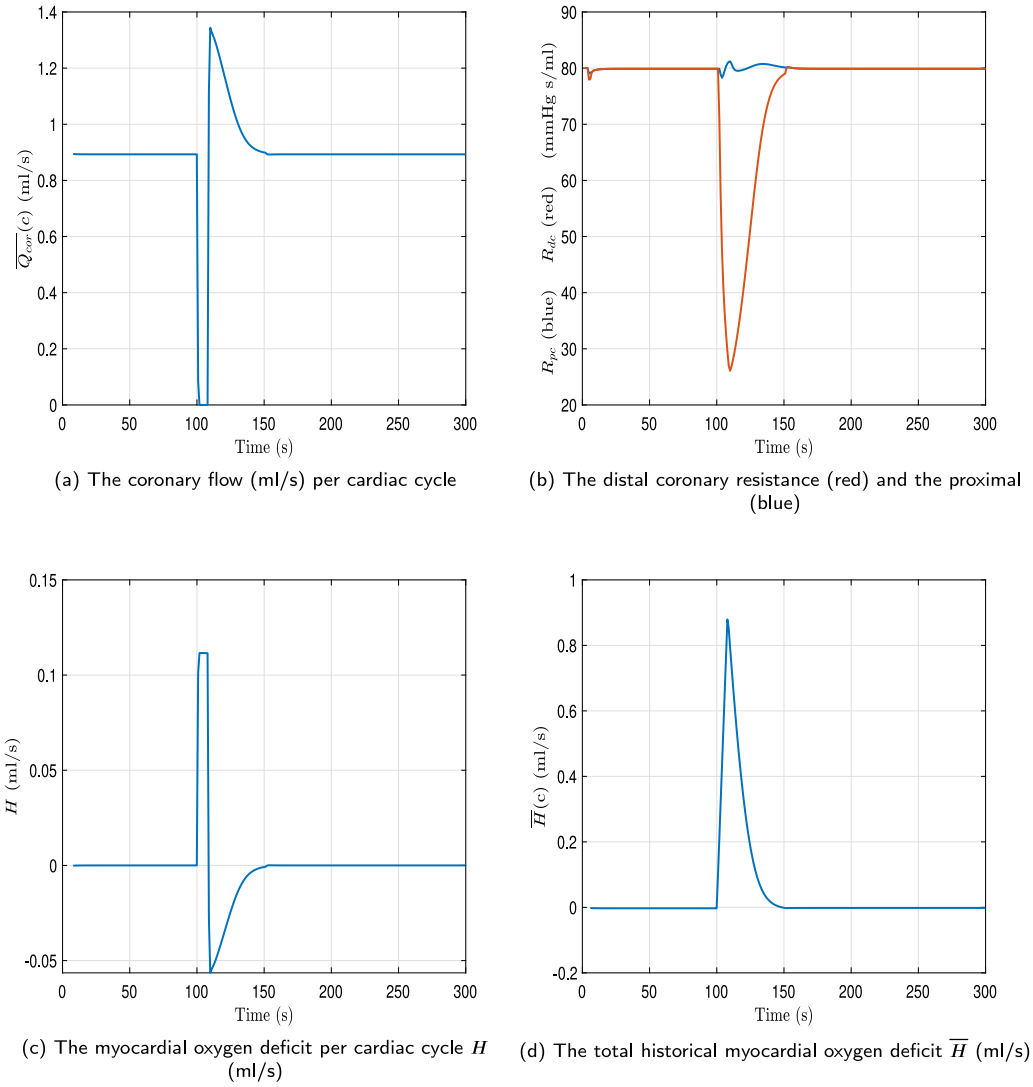

(a) The coronary flow (ml/s) per cardiac cycle

(b) The distal coronary resistance (red) and the proximal (blue)

(c) The myocardial oxygen deficit per cardiac cycle H (ml/s)

(d) The total historical myocardial oxygen deficit $\overline{H}$ (ml/s)

Fig. 7. The controlled response to a reactive hyperemia. A block of the coronary flow occurs at $t = 100$ and lasts for 8 s. The feedback gain $g_b = 15/8$.

did not reproduce the physiological result that the flow following the block removal exceeds that which is incurred during the occlusion period [43,45].

The duration and character of the deficit-supply cycle depends on the feedback gain parameter g_b. A smaller gain results in a longer cycle and this is shown in Fig. 8 for different values of g_b. A gain of $g_b = 15/8$ produces results slightly more comparable to the physiological response shown in figure 2D in [44]. So we use $g_b = 15/8$ in the remainder of this paper. Due to the use of $\overline{H}$ for control, the physiological excess of flow following the block cannot be recreated irrespective of g_b as the supply/demand ratio is driven towards zero regardless of the gain value.

3.6. On-transient exercise using the control model

Using the on-transient exercise regime shown in Fig. 4(a), the controls introduced in Eqs. (27)–(34) are now tested. Fig. 9(a) shows the start and end pressure-volume loops. The final P-V loop is thinner than the first as the loop shifts to the left slightly. Fig. 9(b) reveals though that the stroke volume rises initially for the first 20 to 25 s of exercise before falling, and later starting to recover. This is consistent with one of the four main responses in SV to exercise reported in [39]; generally, the stroke volume increases initially, but later it may continue to rise, plateau, fall, and fall followed by recovering. The SV behaviour here clearly obeys the latter. The reasons for this wide variation are not well understood, but the subject fitness is a good indicator for a continued rise in stroke volume. The SV will be explored further in Section 4. With control, the pump-chart in Fig. 9(c) shows an almost linear rise in mean ventricle pressure and CO, however they both plateau as the HR (Fig. 4(a)) levels out. The linear rise in the pump chart and the outward trajectory towards greater CO and pressure correspond with the expected result from a healthy person during moderate exercise [46]. The increase in mean ventricular pressure displayed in the pump chart is only slight as illustrated in [46]. It shows a rise from approximately 50 mmHg to 60mmHg for a CO rise from 5 L/min to 11 L/min approximately. In our results, the rise in mean pressure is greater, from 40 mmHg to 60 mmHg for a similar rise in CO.

Fig. 10 shows how other heart-performance related measures behave in our proposed control model. The myocardial oxygen demand MVO_2 increases when control is used due to the initial growth in pressure-volume area and the heart rate. Without control the oxygen deficit H increased due to the reduction in coronary flow $Q_{cor}(c)$. With control, a surplus of oxygen is created and H falls along with $\overline{H}$. Feedback resistance control does not play a role during exercise here due to $\overline{H}$ showing a surplus of oxygen.

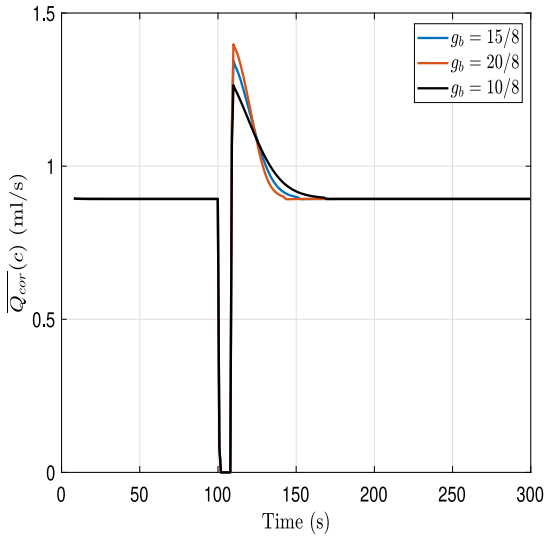

Fig. 8. The effect of the gain parameter f_b in Eq. (28) on the coronary flow during coronary occlusion.

3.7. Off-transient exercise

For off-transient exercise recovery, the final condition and variables from the exercise simulation above (Section 3.6) are used as the initial condition for the recovery test. Exercise recovery is characterised by the heart rate reduction shown in Fig. 4(b). The pressure-volume loop contracts towards the initial shape. The stroke volume recovery is far from smooth, initially rising then falling then rising again above the resting value. The pump-chart (Fig. 11(c)) shows the mean ventricular pressure $\overline{P_v}$ and cardiac output (CO) falling towards the resting condition with a slight overshoot towards the end.

Fig. 12 shows the recovery of various heart-performance stats revealing a 'lumpy' response. The reason for the 'lumpy' response in SV can be traced to the resistance. Although R_{pc} shows a fairly steady recovery, R_{dc} spikes after 100 s. It is found that the uncontrolled off-transient recovery response (shown in Fig. D.1 and D.2 in the Appendix) has a similar 'lumpy' character as the controlled, showing similar patterns at similar times. The character of the recovery may not all be due then to the control regime but caused by the CVS model. This is partly due to the variables a, α_u, k_2, and Ψ being controlled by the heart rate. By the end of the simulation, R_{dc} and R_{pc} continue their slow recovery to their original values.

3.8. The control function gain parameters g_{ff1} and g_{ff2}

The effect of the feedback parameter g_b was explored in Section 3.5. It affects the value of R_{dc} only when the total O_2 deficit is positive. In this section, the effects of the feedforward gain parameters g_{ff1} and g_{ff2} on exercise are explored. Fig. 13 shows the effects of each parameter on the resistance R_{dc} and R_{pc} during on-transient exercise.

It can be seen that g_{ff1} has an almost negligible effect on the behaviour of R_{dc}. R_{pc} is unaffected too. This is due to the parameter aa_1, which has to be changed at the same time as g_{ff1} to set the resting resistance as $R_{dc} = 80$. g_{ff2} does affect the value of the R_{pc} despite the parameter aa_2, with a larger gain causing a greater reduction in R_{pc} during exercise. It does not affect R_{dc}. Neither parameter impacts the stroke-volume strongly though. It was chosen to model the feedforward as the square of the demand. A different exponential function could also have been chosen i.e. $MVO_2(c-1)^3/MVO_2(0)^2$, however it is found (results not shown) that this decreases the stability of the exercise response, causing large fluctuations in behaviour.

3.9. Effects of the heart-rate model parameters λ and υ

So far, the HR model described in Section 2.5 has been used to prescribe the HR using a fixed fitness level $\lambda = 0.85$ and intensity rate $\upsilon = 10$. In this section, the effects of these constants on the exercise control model will be examined. First, the exercise intensity υ is fixed constant at $\upsilon = 10$ and λ is varied between 0.6 and 0.9. Fig. 14 shows the resulting heart rate, stroke volume and pump chart. As can be seen, there is a large gap in the heart rate between $\lambda = 0.6$ and $\lambda = 0.7$. Recall that a female minimum heart rate (40) is used in the HR model. The tests in Fig. 14 use a starting $HR = 60$ bpm; thus, the initial HR falls below the minimum HR when $\lambda = 0.6$, causing the gap between $\lambda = 0.6$ and $\lambda = 0.7$. As λ is reduced, the peak heart rate increases, but is lower for any given time. The stroke volume rises longer using lower values of λ as the heart rate is lower at any given time during the HR rise. It also falls lowest later. Irrespective of the fitness, the peak SV is similar in all responses. The reason will be explored in Section 4. The peak heart rate reached is highest when λ is lowest and the subject is at the lowest fitness. This is consistent with the many physiological studies showing that the fitter the subject the lower the heart rate for any activity level. The pump chart rises further with a lower λ due to the increased heart rate, and the overlapping of the pump chart results show that for the heart rates covered by the range of λs explored (save $\lambda = 0.6$), the model performance agrees well with a healthy person during moderate exercise [46].

In Fig. 15, the effect of the exercise intensity parameter υ on the CVS model is displayed. These results are produced using a fitness $\lambda = 0.85$. The magnitude of the HR rises steadily as υ is increased. When $\upsilon = 18$, the HR (Fig. 15(a)) takes a peculiar shape. This is caused by the HR model approaching maximum ($HR_{max} = 185$), and reflected in the pump chart and stroke volume too. Exercise tests should therefore be kept below an intensity level of $\upsilon = 18$. The severity of the decline in SV is worsened as exercise intensity level is increased. Again, the region of overlapping pump charts and their outward trajectory (towards greater CO and pressure) show that the results correspond well with that of healthy physiological response [46]. The charts deviate away from their outward trajectory only towards the end of the pump chart line, revealing the limits of model.

4. Discussion

In this article, we present a numerical model of the cardiovascular system which captures many of the essential qualities of exercise. The model contains some fundamental differences to previous approaches such as [5,14]. The underlying CVS model accommodates a synergy in that the cellular microscale mechanics are modelled alongside the macro organ scale and the cardiac electrophysiological dynamics. This allows a more detailed analysis and control of the CVS in response to moderate exercise. A particular advantage of the model here, as discussed in Section 1, is that the underlying pressure-volume relationship is not prescribed using the time-varying elastance (TVE) paradigm. As mentioned above, the foundations of the TVE are questionable [16,17] and it prevents or obscures some underlying haemodynamic regulating mechanisms from being modelled. Instead, we embed the mechanics at the microscale within a model of the macroscale. Consequently, the ventricular pressure-volume relationship is developed consistently, allowing a more complete description of the CVS system.

Current approaches to exercise and sports research mainly involves empirical studies, with computational tools used solely for statistical analysis and data collection [47]. Our approach may be used for both sports research, as the heart-rate dynamics are described by a generic exercise intensity and fitness level, but also clinical and academic research, as a more complete description of the CVS system compared to other approaches is provided. This allows the physiological changes and adaptions at the cellular scale to exercise to be investigated. By changing the parameters used in the model, an exercise or sporting

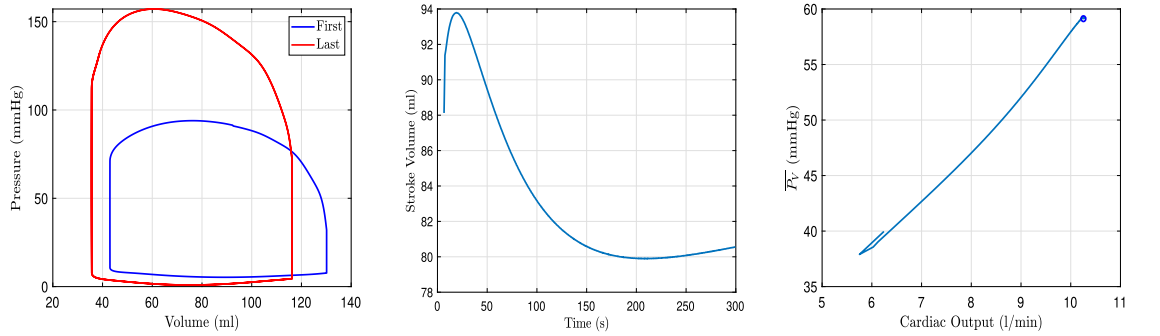

(a) The PV loop at the start (blue) and end (red) of the exercise regime

(b) The controlled stroke volume response

(c) The resulting pump-chart with cardiac control. Marker 'o' shows the line end.

Fig. 9. The behaviour of the model undergoing the exercise regime shown in Fig. 4(a) without cardiac control.

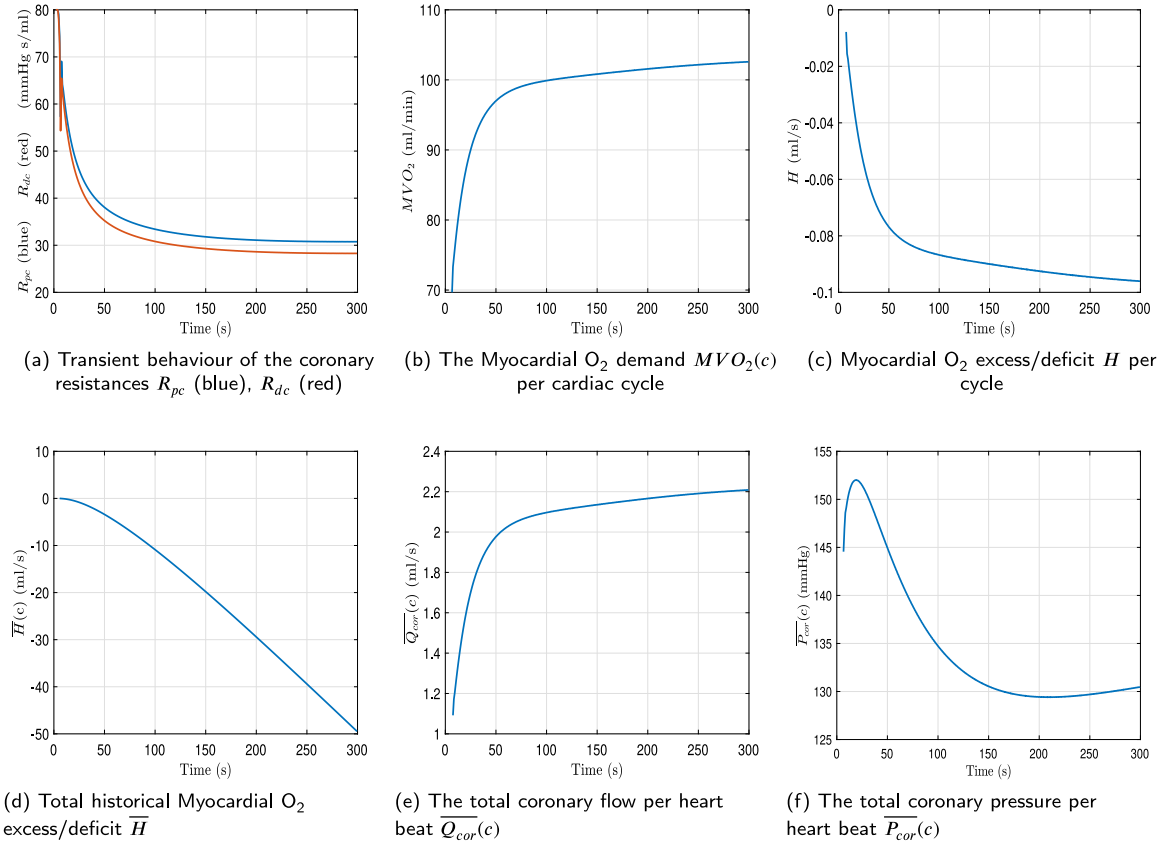

(a) Transient behaviour of the coronary resistances R_{pc} (blue), R_{dc} (red)

(b) The Myocardial O_2 demand $MVO_2(c)$ per cardiac cycle

(c) Myocardial O_2 excess/deficit H per cycle

(d) Total historical Myocardial O_2 excess/deficit $\overline{H}$

(e) The total coronary flow per heart beat $\overline{Q_{cor}}(c)$

(f) The total coronary pressure per heart beat $\overline{P_{cor}}(c)$

Fig. 10. Heart performance measures during controlled exercise (shown in Fig. 4(a)).

activity can be optimised for a specific patient or athlete. This can be achieved without resort to often costly and time consuming empirical studies. For health research and clinical applications, exercise and activity levels can be studied, and used for helping health-care professionals to both understand and tailor drugs and other interventions specific to patient needs. For example, patients suffering from shortness of breath and poor stroke-volume can be prescribed cellular affecting drugs to help increase stroke-volume. Certain activities and sports can be discouraged, whilst others promoted that build on those mechanisms that increase ventricular stroke. Other methods obscure CVS cellular mechanics using a macroscale prescription of the ventricular pressure-volume relationship.

To model exercise, the CVS system is expanded using the coronary and systemic networks by [5] as it allows the pertinent changes to the circulation system to be described. Unlike [5] however, the coronary pressure P_{cor} is not fixed constant, but allowed to adjust accordingly. In Section 3.2, the coronary flow at rest (without exercise) is explored. The double-phase nature characterising the physiological coronary flow waveform is reproduced [5,10,11,41,42] and found to be preserved under exercise conditions [5]. The peak in coronary flow occurs early during ventricular systole, consistent with the previous findings by [10, 41,42]. The effect of the coronary arterial and intramyocardial compliances are explored, in which a larger coronary arterial compliance C_{ac} increases the flow during ventricular diastole, whilst at the same

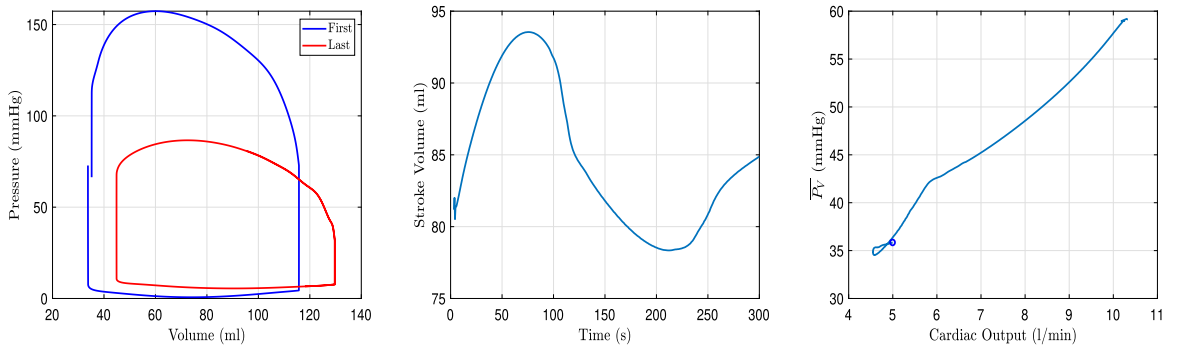

(a) The PV loop at the start (blue) and end (red) of the exercise regime

(b) The controlled stroke volume response

(c) The resulting pump-chart. The marker 'o' shows the end of the test.

Fig. 11. The cardiac behaviour of the exercise regime shown in Fig. 4(b) with cardiac control.

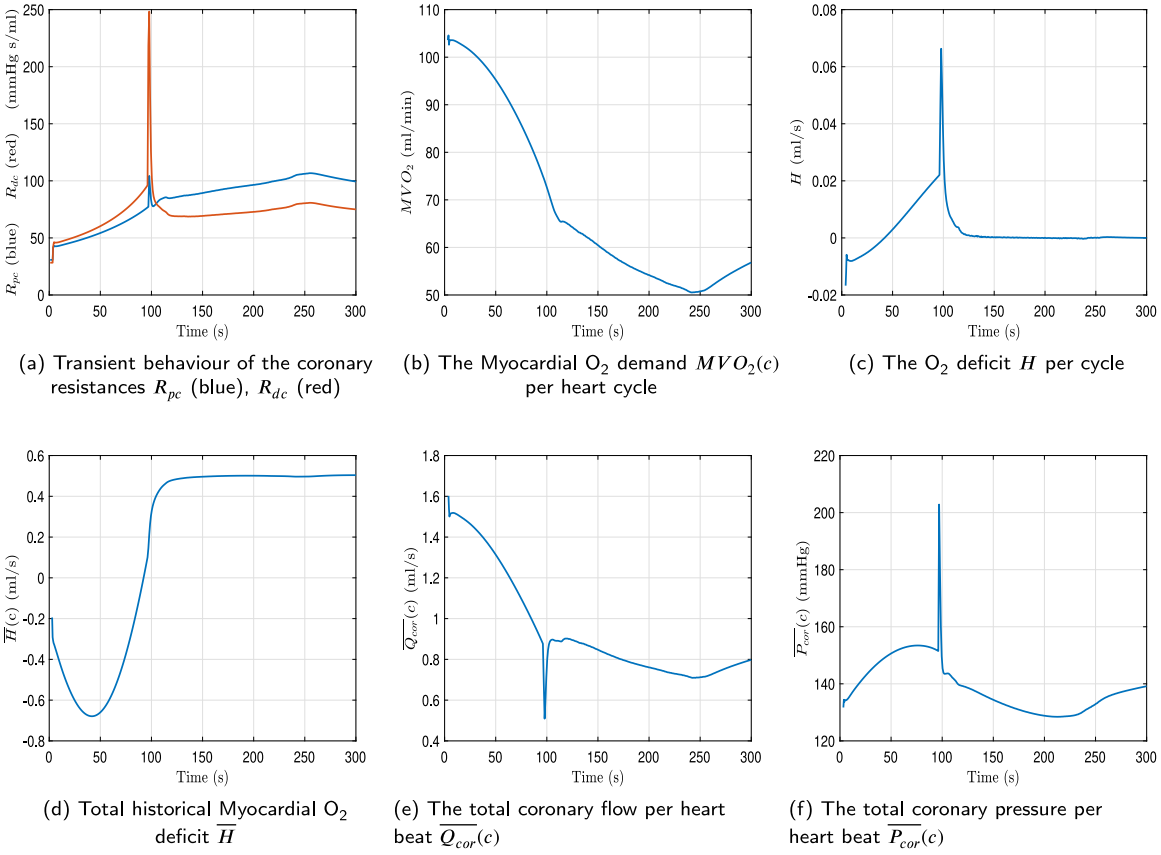

(a) Transient behaviour of the coronary resistances R_{pc} (blue), R_{dc} (red)

(b) The Myocardial O_2 demand $MVO_2(c)$ per heart cycle

(c) The O_2 deficit H per cycle

(d) Total historical Myocardial O_2 deficit $\overline{H}$

(e) The total coronary flow per heart beat $\overline{Q_{cor}}(c)$

(f) The total coronary pressure per heart beat $\overline{P_{cor}}(c)$

Fig. 12. Cardiac performance measures during controlled exercise recovery using the HR shown in Fig. 4(b).

time decreases the systolic flow. The intramyocardial compliance has the opposite effect, where an increased compliance reduces the systolic coronary flow, whilst increasing the diastolic. This pattern is also seen in the numerical results in [10].

Vasodilation of the coronary network is modelled using similar functions as [5]. The distal coronary vessels R_{dc} dilate via both feedback and feedforward messaging. Here, feedback messaging responds to deficits in the oxygen supply, incurred historically or ongoing consistent with physiological behaviour [4,5,15]. Vasodilation of the proximal arteries R_{pc} are modelled using feedforward, 'anticipative' mechanisms, responding to the square of a departure in the myocardial oxygen demand away from operating point values. R_{dc} also contains this feedforward mechanism.

As the microscale mechanics are modelled here alongside the organ-scale, exercise induced changes to the cellular mechanics can be reflected using the control regime, as well as the adjustment of coronary resistances used in most previous exercise explorations. In Eq. (32), the physiological observation that ATP availability increases during exercise [1,2] is represented. Further, Eq. (33) allows the ventricular contraction force to be increased depending on the exercise intensity rate. This intensity-dependent manner in which these two (a and α_u) changes occur [1] is modelled here using the increase/decrease in heart rate, since the heart rate model adopted uses exercise intensity as an

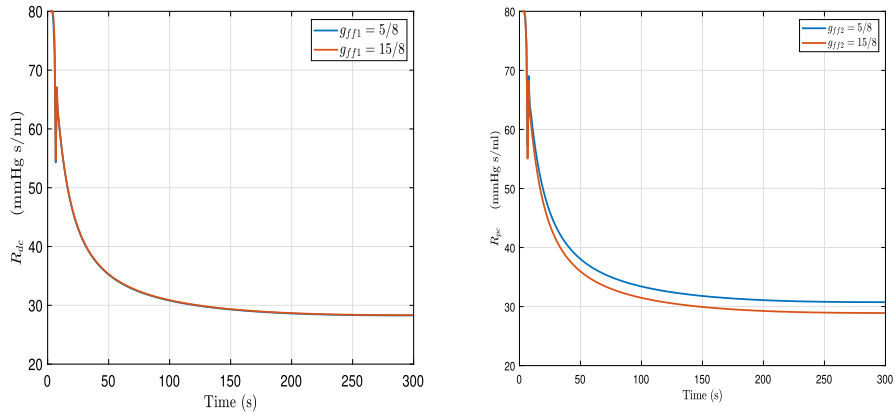

(a) The effect of g_{ff1} on the resistance of R_{dc}. (b) The effect of g_{ff2} on the resistance of R_{pc}.

Fig. 13. The effect of the gain parameters g_{ff1} and g_{ff2} in the coronary resistance control equations during on-transient exercise.

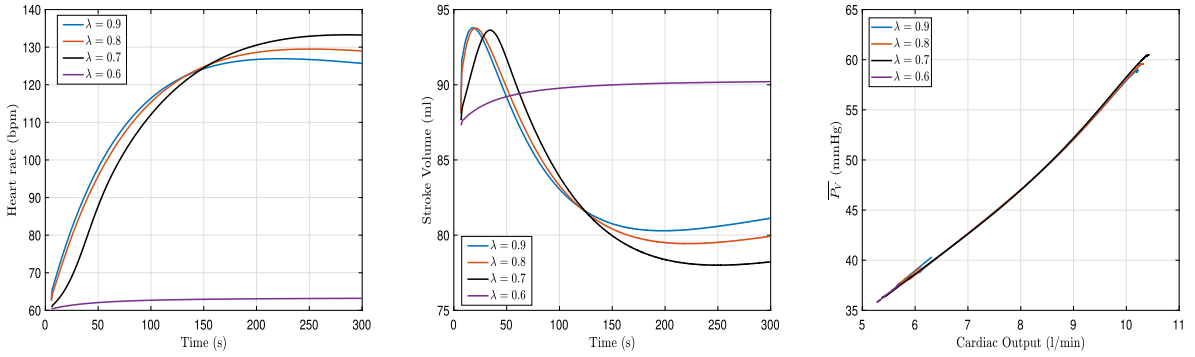

(a) Effect of λ on the heart-rate. (b) The effect of λ on the SV. (c) The effect of λ on the pump chart.

Fig. 14. The effect of the parameter λ in the heart-rate model on the on-transient CVS. For these results, the exercise intensity was fixed at $\upsilon = 10$, $HR(0) = 60$ bps. Blue line: $\lambda = 0.9$, red line: $\lambda = 0.8$, black line: $\lambda = 0.7$, purple line: $\lambda = 0.6$.

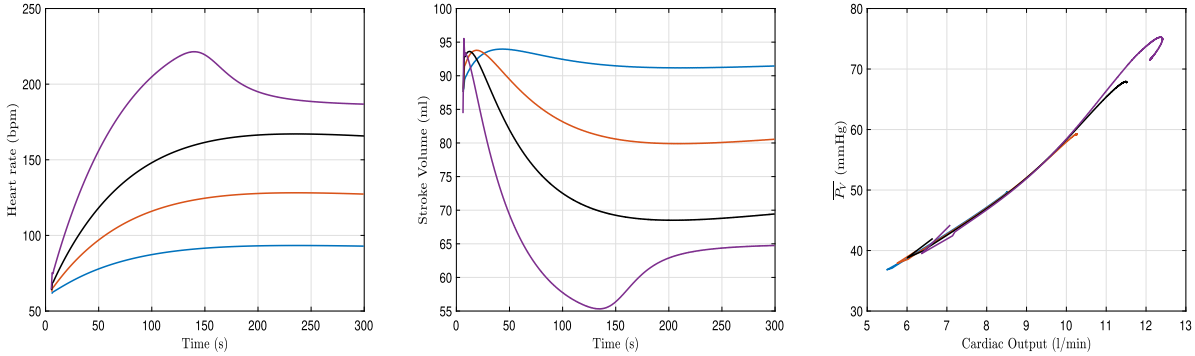

(a) Effect of υ on the HR. (b) Effect of υ on the SV. (c) υ effects on the pump-chart.

Fig. 15. The effect of the exercise intensity parameter υ in the heart-rate model on the on-transient CVS. For these results, the fitness level was fixed at $\lambda = 0.85$, $HR(0) = 60$ bps. Blue line: $\upsilon = 6$, red line: $\upsilon = 10$, black line: $\upsilon = 14$, purple line: $\upsilon = 18$.

input. Future adaptations and improvements to the model may modify these to better reflect the underlying physiological mechanisms.

The heart rate is prescribed using the model provided in [29,30]. This model produces physiological descriptions of the heart rate during both on-transient (starting) and off-transient (recovery) exercise. The model requires just two parameters for input: the exercise intensity, and the subject fitness level. Due to the non-linear behaviour of the electrophysiological model (Section 2.4), the heart rate prescribed using the HR model is over or underestimated by the CVS, so adjustments to the HR model must be made such that the output follows the desired pattern. For simulating exercise, we have use just one exercise intensity level υ and one fitness level ($0 \leq \lambda \leq 1$), however their effects are explored in Section 3.9 showing the changes on the CVS performance.

As an initial test of our proposed exercise control model, we simulate the effect of coronary flow occlusion, in which coronary flow is artificially held zero for a brief period of time. Our simulation of coronary occlusion agrees well with literature [5,43,44]. The agreement with the physiological data can be improved by adjusting the feedback gain parameter f_b. Feedback is the only regulating response as only metabolic demand is affected, in agreement with [5,44]. As the heart rate remains constant during the occlusion, the microscale control functions plays no role in the model response. This response is somewhat intuitive as the CVS cannot 'know' about the occlusion in advance, hence cannot respond in an anticipative, feedforward manner. The model is not, however, able to reproduce the physiological observation that the volume of coronary flow following the occlusion is greater than during flow during block irrespective of the feedback gain.

During on-transient exercise, the cardiac control reduces the coronary resistance at a rate depending on the feedforward gains, as the feedback gain has very little effect. Our resistance control functions are similar to [5] but changes are made after a complete heart cycle rather than continuously in time. Were adjustments made using the latter method, the coronary resistance and CVS parameters will fluctuate during any particular heart beat, while the heart rate at the end of any particular beat cycle would be faster (or slower) than the rate at the start. The method used here is, however, more desirable to ensure stability. The myocardial oxygen demand MVO_2 rises during exercise, but so too does the coronary flow, causing an oxygen surplus (negative H). The feedback method used here only responds to a deficit. The stroke volume increases initially during on-transient exercise with the length depending on the fitness and exercise intensity. It then falls, followed by recovering as the HR plateaus. This behaviour is consistent with one of the four main physiological responses in SV [39].

In Section 3.9 the effect of the HR model parameters υ and λ on the CVS system is explored. These two variables are the only input values required for any exercise simulation. It can be seen using these results that exercise routines can be matched to given fitness levels. In Fig. 16, the stroke volume is plotted against the demand MVO_2 for different values of λ showing that the peak SV is similar between cases (the lowest value of λ shows a slight reduction) and occurs at the same value of MVO_2. These results agree well with one of the 4 main responses in SV to exercise [39]. The level of oxygen demand MVO_2 when the maximum SV occurs is unaffected in our model for any given fitness level, so the maximum SV occurs at the same value of MVO_2 irrespective of fitness level. The fitness level however is a good indicator for the value of this level of MVO_2 [39], so future modifications to the model should therefore aim to link the level of MVO_2 at which maximum SV occurs to the fitness level. A limit on exercise intensity ($\upsilon < 18$) is found for a given fitness level, as the HR behaves unphysiologically. This is partly due to the maximum HR predicted using the underlying HR model being approached ($HR_{max} = 185$ [29,30]), and partly due to the non-linear electro-mechanical model. The SV rises for longer using lower fitness and exercise intensity, but reaches the same peak value. This is clearly due to the HR being lower until $HR = 150$ using lower fitness and exercise intensity. Again, future adaptations to the model should therefore aim to link the peak in SV to the fitness.

Finally, to demonstrate one of the utilities of our model in future, we comment on the microscale mechanics. Using the on-transient exercise results presented in Section 3.6, we show in Fig. 17 the pressure-volume loop (Fig. 9(a)) equivalent of the cardiac myofibers, that is the stretch ϵ_c against the force developed $\tau_c d_0$. The myofiber force increases for the first half of the simulation, then remains at the same level for the remainder. The stretch rises for the first 20 to 25 s, but then declines slightly for the remainder of the simulation. The force results correspond to the mean ventricular pressure, which increases initially before plateauing. The cell stretching corresponds to the stroke volume. In this way, we can see the correspondence between the cellular mechanics and whole organ activity. Thus, using our model allows dysfunction of

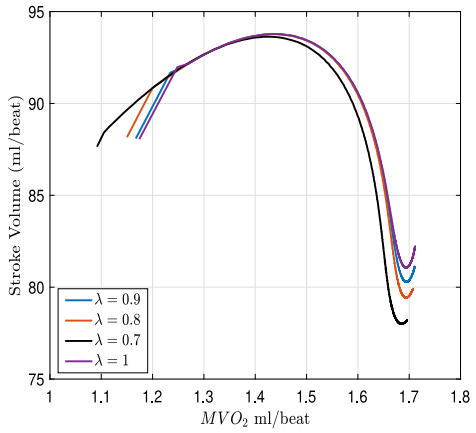

Fig. 16. The stroke volume against the oxygen demand MVO_2 for different levels of fitness.

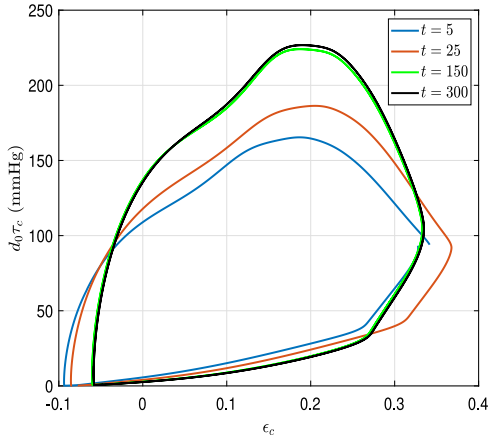

Fig. 17. The stress–strain loops at different times for the simulation results shown in Section 3.6.

microscale dynamics to be traced relatively easily using measurements of heart performance during physical activity. Given the difficulty in measuring the microscale dynamics in vivo, this will be of great use in the diagnosis of diseases.

The study presented in this paper can be further extended in future works in several ways. First, while the use of the heart rate for the microscale control functions is useful, it will be ideal to develop a more physiologically representative model of the biological processes involved, although this will require significant research since these processes are currently not well understood. That is, more empirical investigation is necessary to elucidate the actual biological mechanisms to begin with. The model can also be further developed to reproduce the link between the fitness of the individual and the behaviour of this O_2 demand level, so that the fitter the person the greater the demand level at which the SV begins to decline [39], which was not portrayed from our model. Another direction of future work would be to make the model flexible by developing a robust, systematic method of identifying the values of parameters (e.g. by using machine learning, or neural network) in different scenarios.

Another direction for future work will be to remove our model assumption that the sarcomeres making up any myofiber behave as single unit since in reality, the behaviour of any myofiber is dominated by non-uniformities of sarcomere; especially when biological variability

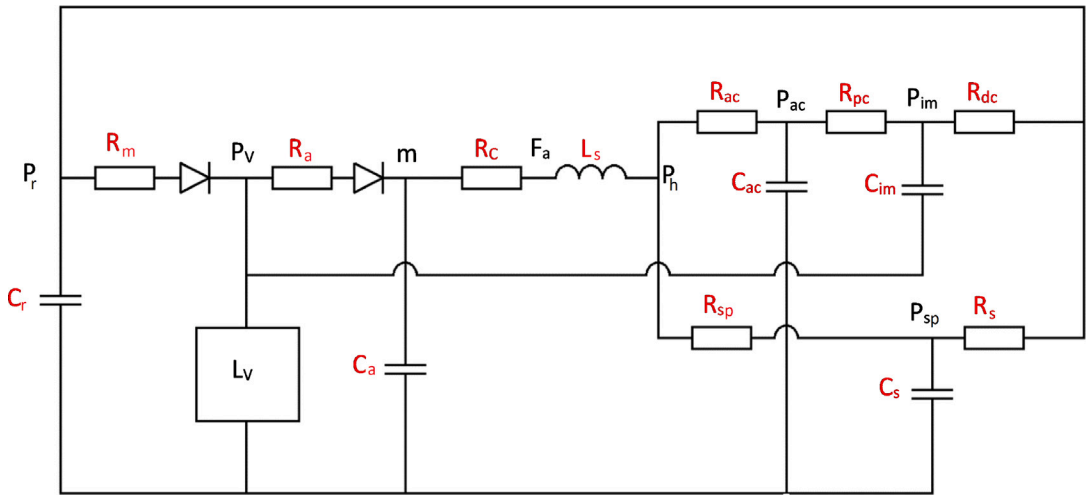

Fig. A.1. The electrical-equivalent diagram of the complete cardio-vascular system model. L_v stands for left ventricle, R and C are the resistance and compliance elements respectively, and L_s is an inductor for the aortic blood inertance. The value and physiological meaning of each element can be found in Table 2. The diodes in Fig. 16 represent the aortic and mitral valves. Biologically these valves ensure that fluid flow between heart compartments is only one-way and prevent flow 'downstream' affecting the upstream blood flow. Mathematically, the valve function is expressed by the Heaviside operations (subscript +) in Eqs. (12), (13), and (18). The Heaviside function selects only positive values of the terms for which it is used.

and fluctuations are taken into account. Hence, as detailed by [48], microscale sarcomere regulation may not necessarily lead to expected macroscale outcomes. In their model, a myofiber is treated as an ensemble of individual sarcomere, and build in biological variability and length fluctuations. Their myofibril model can predict experimental observations such as muscle creep and length redistribution that cannot be predicted by models that assume isometric conditions. They also show how an accumulation of overstretched sarcomeres leads to muscle damage. In order for our model to reflect realistic conditions therefore, an extension to spatio-temporal dimensions would be needed as well as changes to our microscale model. This would also enable wave propagation in length to be investigated. Again, this is left for future work.

5. Conclusion

The aim of this article is to develop a synergistic low-order, CVS model that includes the coronary network and the various control mechanisms for modelling exercise. It is tested using a physiologically accurate representation for on-transient and off-transient exercising heart-rate. The coronary network used by [5] is adopted to allow a relatively compact representation of different parts of the network. Our model successfully reproduces the two-phase character of the coronary flow. Feedforward and feedback resistance control functions are then implemented and their effects tested by simulating reactive hyperemia. Results show a physiologically accurate reproduction of the coronary flow response. An advantage of using the underlying synergistic model is that it allows other cardiac performance related control functions to be tested. We therefore use simple feedforward functions to increase ATP [1–3,36] during exercise, increase the stress generated by the cardiac myofibers [1], and increase the stroke volume [39] without substantially modifying the ESV [1]. Simulations of both on and off-transient exercise produce results comparable with physiological behaviour. In particular, an overlapping region on the pump chart reveals that for the range of heart rates explored in this study, the response corresponds to that of a healthy person during moderate exercise. The model is compact and intuitive requiring just two input values: exercise intensity level and subject fitness level. A further advantage of the synergistic CVS model is demonstrated in the discussion in the correspondence between exercise performance and the mechanics of the myofibers.

CRediT authorship contribution statement

Nicholas F. Pearce: Conceptualization, Methodology, Formal analysis, Writing. **Eun-jin Kim:** Conceptualization, Methodology, Writing, Supervision.

Declaration of competing interest

The authors declare no conflict of interest.

Appendix A. The CVS model

In Fig. A.1, the electrical-equivalent diagram of the complete cardio-vascular system model is shown. L_v stands for left ventricle, R and C are the resistance and compliance elements respectively, and L_s is an inductor for the aortic blood inertance.

Appendix B. Steady state resting heart (control) results

The results for the CVS model at rest, with a steady heart rate of 1 bps, and free of pathologies is shown in Fig. B.1. In Fig. B.2, the steady-state pressure-volume loops are shown with different preloads. The line gives the end-systolic pressure-volume relationship (ESPVR), showing the maximum ventricle pressure at any volume. See Section 3.1 for further details.

Appendix C. Heart rate model

The heart rate model during exercise used in this report is that provided by [29,30]. Readers are referred to these papers for further details. The main equations and parameters are provided below for completeness. In the following, HR is the heart rate (bps).

$$\frac{dHR}{dt}(HR, HR(0), \lambda, \upsilon, t) = -f_{min} f_{max} f_D \tag{35}$$

where υ is the exercise intensity, $HR(0)$ is the initial HR, λ is the fitness level, and t is time. f_{max} and f_{min} control the dynamics near the maximum and minimal heart rate respectively, and f_D controls the

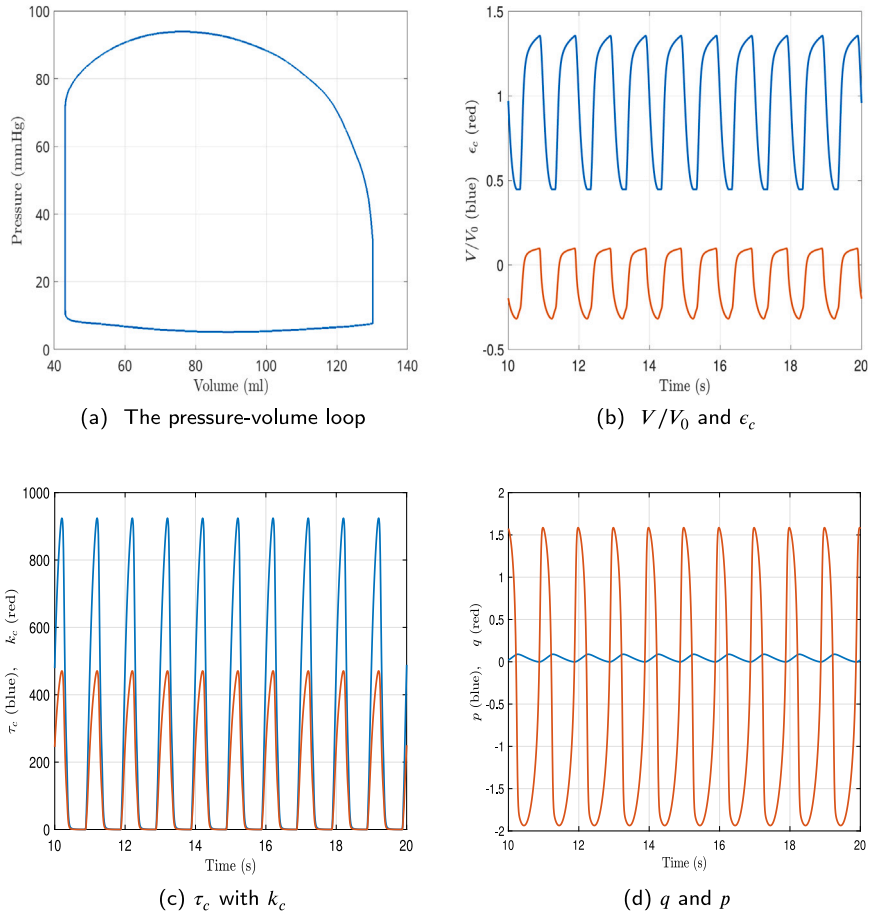

(a) The pressure-volume loop (b) V/V_0 and ϵ_c

(c) τ_c with k_c (d) q and p

Fig. B.1. The steady state resting ventricular case results at rest. Fig. B.1(a) shows the (steady) pressure-volume loop, Fig. B.1(b) shows V/V_0 with ϵ_c, Fig. B.1(c) shows τ_c with k_c, and Fig. B.1(d) shows q with p.

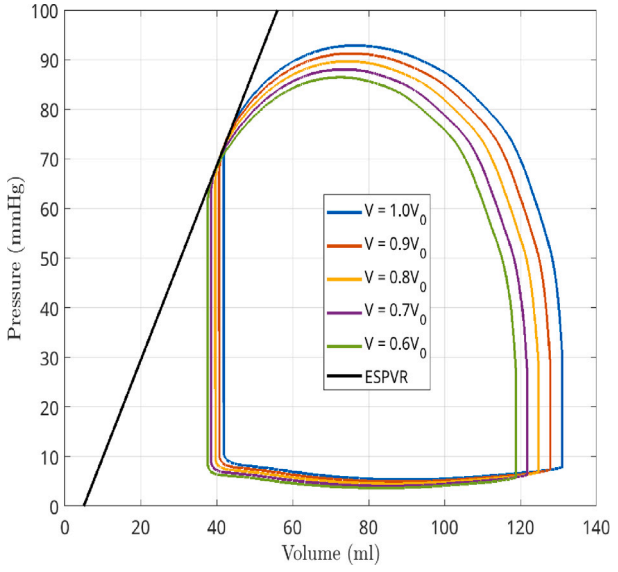

Fig. B.2. Steady state pressure-volume loops for different preloads $V(0) = [1.0, 0.9.0.8, 0.7, 0.6]V_0$: The black line shows the ventricular ESPVR for the resting steady state case results. The ESPVR line shows the maximum ventricular pressure developed at any volume.

dynamics near the bodies heart rate demand D. These functions are given below.

$$f_{max}(HR) = -\left\{1 - e^{-\left(\frac{HR-HR_{max}}{10}\right)^2}\right\}, \tag{36}$$

$$f_{min}(HR, \lambda) = \left\{1 - e^{-\left(\frac{HR-HR_{min}}{10}\right)^2}\right\}, \tag{37}$$

$$f_D(HR; HR(0); v; \lambda; t) = -d(\lambda)[HR - D(\lambda, v, t)], \tag{38}$$

where $d(\lambda)$ controls the dynamics very near the oxygen demand D. Further parameters used to model the HR are given below

$$HR_{min} = \frac{35}{\lambda}, \tag{39}$$

$$HR_{min} = \frac{35}{\lambda} + 5, \tag{40}$$

$$HR_{max} = 185, \tag{41}$$

$$L_{basal} = 1, \tag{42}$$

$$L_{max} = 12 \tag{43}$$

As males have been found to have a lower resting heart rate than females (+5 bpm approximately), two minimum heart rates are provided in the HR model [29,30]. Eq. (39) is the male minimum HR, and Eq. (40) is the female minimum HR, and Eq. (40) is used in this paper. HR_{max} is the maximum HR irrespective of gender, L_{basal} is the basal lactose level, and L_{max} is the maximum lactose level. Further,

$$d(\lambda) = 0.01\lambda, \tag{44}$$

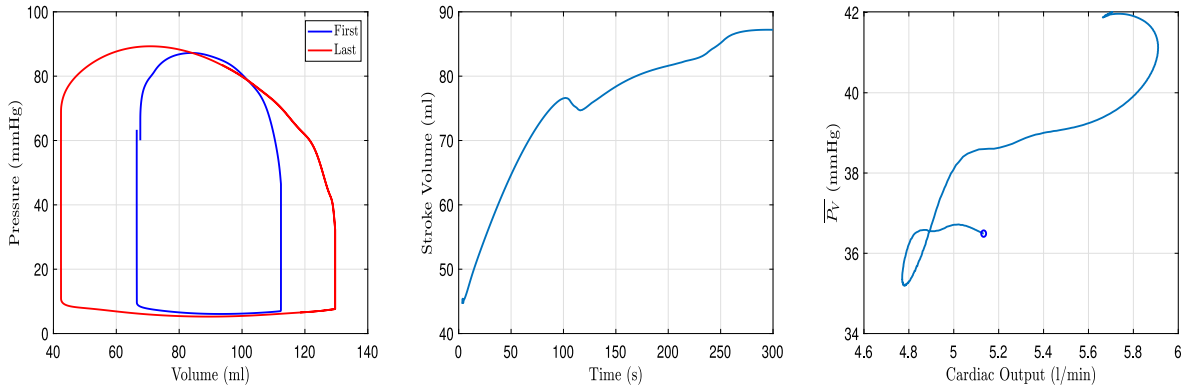

(a) The PV loop at the start (blue) and end (red) of the exercise regime

(b) The uncontrolled stroke volume response

(c) The resulting pump-chart without cardiac control

Fig. D.1. The cardiac behaviour of the exercise regime shown in Fig. 4(b) without cardiac control.

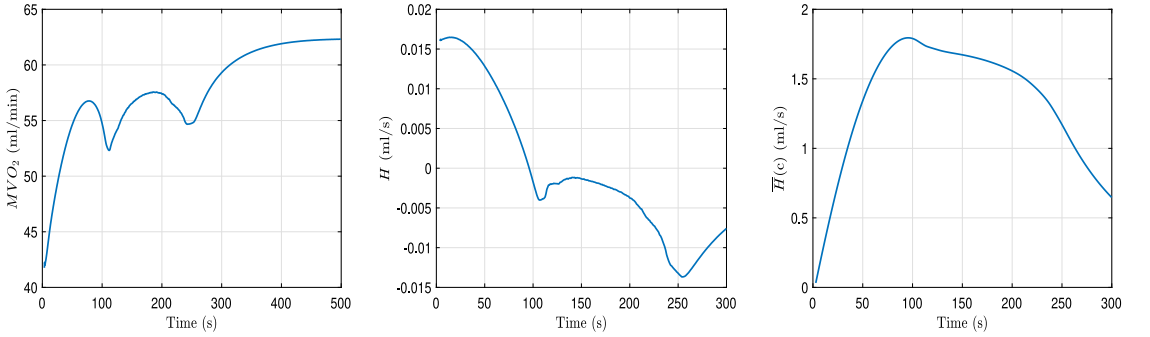

(a) Total Myocardiac O_2 demand $MVO_2(c)$ per cardiac cycle

(b) Myocardiac O_2 deficit H per cycle

(c) Total historical Myocardiac O_2 deficit $\overline{H}$

Fig. D.2. Cardiac measures during off-transient exercise recovery (shown in Fig. 4(b)) without cardiac control.

$$D(v,\lambda,t) = \hat{D}(\lambda,v,t) + \{HR(0) - \hat{D}(\lambda,v,t)\}e^{-\sigma t^2}, \tag{45}$$

$$\hat{D} = D_{ss}(v,\lambda,t) + D_{LA}(v,\lambda,t), \tag{46}$$

$$D_{LA}(v,\lambda,t) = 4L(\lambda,v,t), \tag{47}$$

$$D_{ss} = \frac{v}{v_{max}}(HR_{max} - HR_{min}) + HR_{rest}, \tag{48}$$

$$\sigma = 0.003\lambda\left(\frac{HR_{max} - HR_{min}}{HR(0) - HR_{min}}\right)^4, \tag{49}$$

$$L(\lambda,v) = L_{basal} + (L_{max} - L_{basal})\exp\{0.5[v - v_{max}(\lambda)]\}, \tag{50}$$

$$v_{max} = 20\sqrt{\lambda} \tag{51}$$

$\hat{D}$ is the maximum demand, D_{ss} and D_{LA} are the steady-state and lactose induced demands respectively, and finally L is the lactose level.

Appendix D. Off-transient recovery response without control

For the uncontrolled response to exercise recovery, the final values of different variables and parameters taken at the end of the uncontrolled exercise test are used as the initial condition. The results are shown in Fig. D.1 together with Fig. D.2 shows some heart-performance measures.

References

[1] L. Xiang, R. Hester, Cardiovascular responses to exercise, in: Colloquium Series on Integrated Systems Physiology: From Molecule to Function, Vol. 3, 2011, pp. 1–124, http://dx.doi.org/10.4199/C00040ED1V01Y201109ISP027.

[2] J. González-Alonso, D.B. Olsen, B. Saltin, Erythrocyte and the regulation of human skeletal muscle blood flow and oxygen delivery: Role of circulating ATP, Circ. Res. 91 (11) (2002) 1046–1055.

[3] J.C. Arciero, B.E. Carlson, T.W. Secomb, Theoretical model of metabolic blood flow regulation: Roles of ATP release by red blood cells and conducted responses, Am. J. Physiol.-Heart Circulat. Physiol. (2008).

[4] E.O. Feigl, Neural control of coronary blood flow, J. Vasc. Res. 35 (2) (1998) 85–92.

[5] C.J. Arthurs, K.D. Lau, K.N. Asrress, S.R. Redwood, C.A. Figueroa, A mathematical model of coronary blood flow control: Simulation of patient-specific three-dimensional hemodynamics during exercise, Am. J. Physiol.-Heart Circulat. Physiol. 310 (9) (2016) H1242–H1258.

[6] M.W. Gorman, J.D. Tune, K.N. Richmond, E.O. Feigl, Feedforward sympathetic Coronary vasodilation in exercising dogs, J. Appl. Physiol. 89 (5) (2000) 1892–1902.

[7] J.D. Tune, K.N. Richmond, M.W. Gorman, E.O. Feigl, Control of Coronary blood flow during exercise, Exper. Biol. Med. 227 (4) (2002) 238–250.

[8] J.D. Tune, M.W. Gorman, E.O. Feigl, Matching Coronary blood flow to myocardial oxygen consumption, J. Appl. Physiol. 97 1 (2004) 404–415.

[9] C.A. Taylor, T.A. Fonte, J.K. Min, Computational fluid dynamics applied to cardiac computed tomography for noninvasive quantification of fractional flow reserve: Scientific basis, J. Am. Coll. Cardiol. 61 (22) (2013) 2233–2241.

[10] S. Mantero, R. Pietrabissa, R. Fumero, The coronary bed and its role in the cardiovascular system: A review and an introductory single-branch model, J. Biomed. Eng. 14 (2) (1992) 109–116.

[11] Z. Duanmu, M. Yin, X. Fan, X. Yang, X. Luo, A patient-specific lumped-parameter model of Coronary circulation, Sci. Rep. 8 (1) (2018) 1–10.

[12] O. Barnea, Mathematical analysis of coronary autoregulation and vascular reserve in closed-loop circulation, Comput. Biomed. Res. 27 (4) (1994) 263–275.

[13] E. Magosso, M. Ursino, Cardiovascular response to dynamic aerobic exercise: A methematical model, Med. Biol. Eng. Comput. 40 (6) (2002) 660–674.

[14] H.J. Kim, K. Jansen, C. Taylor, Incorporating autoregulatory mechanisms of the cardiovascular system in three-dimensional finite element models of arterial blood flow, Ann. Biomed. Eng. 38 (7) (2010) 2314–2330.
[15] J. Miyashiro, E. Feigl, A model of combined feedforward and feedback control of Coronary blood flow, Am. J. Physiol.-Heart Circulat. Physiol. 268 (2) (1995) H895–H908.
[16] T.E. Claessens, D. Georgakopoulos, M. Afanasyeva, S.J. Vermeersch, H.D. Millar, N. Stergiopulos, N. Westerhof, P.R. Verdonck, P. Segers, Nonlinear isochrones in murine left ventricular pressure-volume loops: How well does the time-varying elastance concept hold? Am. J. Physiol.-Heart Circulat. Physiol. 290 (4) (2006) H1474–H1483.
[17] A. Pironet, P.C. Dauby, S. Paeme, S. Kosta, J.G. Chase, T. Desaive, Simulation of left atrial function using a multi-scale model of the cardiovascular system, PLoS One 8 (6) (2013) e65146.
[18] E.J. Kim, M. Capoccia, Synergistic model of cardiac function with a heart assist device, Bioengineering 7 (1) (2019) 1.
[19] E.J. Kim, M. Capoccia, Mechano-electric effect and a heart assist device in the synergistic model of cardiac function, Math. Biosci. Eng. 17 (5) (2020) 5212–5233.
[20] N. Pearce, E.j. Kim, Modelling the cardiac response to a mechanical stimulation using a low-order model of the heart, Math. Biosci. Eng. 18 (4) (2021) 4871–4893.
[21] G. Tse, S.T. Wong, V. Tse, Y.T. Lee, H.Y. Lin, J.M. Yeo, Cardiac dynamics: Alternans and arrhythmogenesis, J. Arrhythmia 32 (5) (2016) 411–417.
[22] P. Colli Franzone, L.F. Pavarino, S. Scacchi, Effects of mechanical feedback on the stability of cardiac scroll waves: A bidomain electro-mechanical simulation study, Chaos 27 (9) (2017) 093905, http://dx.doi.org/10.1063/1.4999465, arXiv:10.1063/1.4999465.
[23] P. Kohl, P. Hunter, D. Noble, Stretch-induced changes in heart rate and rhythm: Clinical observations, experiments and mathematical models, Prog. Biophys. Mol. Biol. 71 (1) (1999) 91–138.
[24] A. Collet, J. Bragard, P. Dauby, Temperature, geometry, and bifurcations in the numerical modeling of the cardiac mechano-electric feedback, Chaos 27 (9) (2017) 093924.
[25] N. Pearce, E.J. Kim, An investigation of left ventricular valve disorders and the mechano-electric feedback using a synergistic lumped parameter cardiovascular numerical model, Bioengineering 9 (9) (2022) http://dx.doi.org/10.3390/bioengineering9090454, URL https://www.mdpi.com/2306-5354/9/9/454.
[26] D. Roy, O. Mazumder, A. Sinha, S. Khandelwal, Multimodal cardiovascular model for hemodynamic analysis: Simulation study on mitral valve disorders, Plos One 16 (3) (2021) e0247921.
[27] P. Lancellotti, T. Marwick, L.A. Pierard, How to manage ischaemic mitral regurgitation, Heart 94 (11) (2008) 1497–1502.
[28] M.B. Bastos, D. Burkhoff, J. Maly, J. Daemen, C.A. den Uil, K. Ameloot, M. Lenzen, F. Mahfoud, F. Zijlstra, J.J. Schreuder, et al., Invasive left ventricle pressure–volume analysis: Overview and practical clinical implications, Eur. Heart J. 41 (12) (2020) 1286–1297.
[29] M.S. Zakynthinaki, Modelling heart rate kinetics, PLOS ONE 10 (4) (2015) 1–26, URL.
[30] M.S. Zakynthinaki, Simulating heart rate kinetics during incremental and interval training, Biomed. Hum. Kinetics 8 (1) (2016) 144–152.
[31] J. Bestel, Modèle différentiel de la contraction musculaire contrôlée: Application au système cardio-vasculaire (Ph.D. thesis), Paris 9, 2000.
[32] J. Bestel, F. Clément, M. Sorine, A biomechanical model of muscle contraction, in: International Conference on Medical Image Computing and Computer-Assisted Intervention, Springer, 2001, pp. 1159–1161.
[33] D.A. Rowen, A.D. Likens, N. Stergiou, Revisiting a classic: Muscles, reflexes, and locomotion by McMahon, J. Biomech. Gait Anal. (2020) 149–224.
[34] P. Krejci, J. Sainte-Marie, M. Sorine, J. Urquiza, Modelling and simulation of an active fibre for cardiac muscle, in: Submitted to Biomechanics and Modelling in Mechanobiology, Citeseer, 2006.
[35] R. FitzHugh, Impulses and physiological states in theoretical models of nerve membrane, Biophys. J. 1 (6) (1961) 445–466.
[36] E. Hultman, P. Greenhaff, Skeletal muscle energy metabolism and fatigue during intense exercise in man, Sci. Progr. (1933-) (1991) 361–370.
[37] J. Stirling, M. Zakynthinaki, B. Saltin, A model of oxygen uptake kinetics in response to exercise: Including a means of calculating oxygen demand/deficit/debt, Bull. Math. Biol. 67 (5) (2005) 989–1015, http://dx.doi.org/10.1016/j.bulm.2004.12.005, URL https://www.sciencedirect.com/science/article/pii/S009282400500008X.
[38] T. Kameyama, H. Asanoi, S. Ishizaka, K. Yamanishi, M. Fujita, S. Sasayama, Energy conversion efficiency in human left ventricle, Circulation 85 (3) (1992) 988–996.
[39] C.A. Vella, R.A. Robergs, A review of the stroke volume response to upright exercise in healthy subjects, Br. J. Sports Med. 39 (4) (2005) 190–195, http://dx.doi.org/10.1136/bjsm.2004.013037, arXiv:https://bjsm.bmj.com/content/39/4/190.full.pdf.
[40] M.A. Simaan, A. Ferreira, S. Chen, J.F. Antaki, D.G. Galati, A dynamical state space representation and performance analysis of a feedback-controlled rotary left ventricular assist device, IEEE Trans. Control Syst. Technol. 17 (1) (2008) 15–28.
[41] J.I. Hoffman, B. GD, Transmural variations in myocardial perfusion, 1976.
[42] J. Spaan, N. Breuls, J.D. Laird, Diastolic-systolic coronary flow differences are caused by intramyocardial pump action in the anesthetized dog, Circ. Res. 49 (3) (1981) 584–593.
[43] M. Marcus, C. Wright, D. Doty, C. Eastham, D. Laughlin, P. Krumm, C. Fastenow, M. Brody, Measurements of Coronary velocity and reactive hyperemia in the coronary circulation of humans, Circ. Res. 49 (4) (1981) 877–891.
[44] A.G. Goodwill, G.M. Dick, A.M. Kiel, J.D. Tune, Regulation of coronary blood flow, Comprehens. Physiol. 7 (2) (2017) 321.
[45] R.A. Olsson, Myocardial reactive hyperemia, Circ. Res. 37 (3) (1975) 263–270.
[46] N. Westerhof, N. Stergiopulos, M.I. Noble, B.E. Westerhof, et al., Snapshots of hemodynamics: an aid for clinical research and graduate education, Vol. 7, Springer, 2010.
[47] C. Gratton, I. Jones, Research Methods for Sports Studies, Taylor & Francis, 2010.
[48] S. Givli, K. Bhattacharya, A coarse-grained model of the myofibril: Overall dynamics and the evolution of sarcomere non-uniformities, J. Mech. Phys. Solids 57 (2) (2009) 221–243, http://dx.doi.org/10.1016/j.jmps.2008.10.013, URL https://www.sciencedirect.com/science/article/pii/S0022509608001907.